Water Air Soil Pollut (2026) 237:1060
https://doi.org/10.1007/s11270-026-09719-3

Gamma Radiation–Induced Synthesis of Pectin/Arabic Gum-Based Nanocomposite Hydrogels for Enhanced Water Remediation

Asmaa Sayed · D. M. Aboelkhir · Razan Mohamed · Ayman Amin · Ghada A. Mahmoud

Received: 17 March 2026 / Accepted: 27 June 2026

Abstract Industrial dye contamination represents a major environmental concern, necessitating efficient and sustainable remediation strategies. In this study, a CuO@pectin/Arabic gum-g-diethylaminoethyl methacrylate (CuO@pectin/Arabic gum-g-DEAEMA) nanocomposite hydrogel was developed via gamma irradiation–induced copolymerization, providing a clean and initiator-free synthesis route. Successful incorporation of CuO nanoparticles was confirmed by DLS, EDX, and XRD analyses, while TGA demonstrated enhanced thermal stability. SEM observations revealed a rough and wrinkled surface morphology favorable for dye adsorption. BET analysis further showed that CuO incorporation increased the surface area from 14.05 to 28.22 m^2 g^{-1} and the total pore volume from 0.08685 to 0.2201 cm^3 g^{-1}, confirming improved porosity and accessibility of adsorption sites. Adsorption studies showed that methylene blue (MB) removal follows a pseudo-second-order kinetic model, indicating chemisorption, while the Freundlich isotherm suggests heterogeneous multilayer adsorption. The CuO-containing hydrogel exhibited significantly improved adsorption performance compared with the pristine system. In addition, the nanocomposite demonstrated antibacterial activity against Gram-positive bacteria, indicating potential resistance to biofouling. The developed hydrogel combines green synthesis, enhanced porosity, improved adsorption efficiency, and multifunctional performance, making it a promising candidate for sustainable wastewater treatment applications.

Keywords Biohydrogel · Arabic gum · Pectin · Gamma irradiation · MB dye removal

1 Introduction

Water is essential for the survival of all living organisms; however, its contamination by various pollutants has become a critical environmental challenge worldwide (Ali et al., 2026). Industrialization and urbanizati on have significantly increased the discharge of hazardous substances into water bodies, arising from both point and non-point sources, thereby threatening ecosystems and human health (Raza et al., 2026). Among these pollutants, organic dyes represent a particularly problematic class due to their complex aromatic structures, high stability, and resistance to biodegradation (Sayed et al., 2025a). Dyes are extensively used in textile, paper, cosmetic, and pharmaceutical

A. Sayed (✉) · D. M. Aboelkhir · G. A. Mahmoud
Polymer Chemistry Department, National Center for Radiation Research and Technology, Egyptian Atomic Authority Cairo, Cairo, Egypt
e-mail: asmaasayedncrrt@gmail.com

R. Mohamed
Faculty of Biotechnology, October University for Modern Sciences and Arts (MSA), Giza, Egypt

A. Amin
Faculty of Agriculture, Cairo University, Cairo, Egypt

Published online: 11 July 2026

industries, leading to the release of large volumes of colored effluents into aquatic systems (Mahmoud et al., 2023). These compounds not only reduce light penetration and inhibit photosynthesis but also exhibit toxic, mutagenic, and carcinogenic effects (Al-Mur & Jamal, 2026). Methylene blue (MB), a widely used cationic dye, is commonly applied in dyeing processes and medical treatments; however, its excessive accumulation in wastewater can cause severe health issues, including respiratory problems, eye irritation, and gastrointestinal disturbances. Therefore, the development of efficient and sustainable strategies for dye removal is of paramount importance (Fakry et al., 2026).

Various treatment technologies have been explored for dye removal, including physical, chemical, and biological methods. Among these, adsorption has emerged as one of the most effective and economically feasible approaches due to its simplicity, high efficiency, and operational flexibility. The performance of adsorption systems is largely governed by the properties of the adsorbent material, particularly surface area, porosity, and the presence of functional groups.

Hydrogels have gained significant attention as versatile adsorbents due to their high swelling capacity, porosity, and ability to host functional groups that interact with pollutants (Abdel-Raouf et al., 2023). Among various hydrogel-forming materials, Arabic gum and pectin are widely used biopolymers known for their biodegradability**,** renewability, and eco-friendliness (Sabry et al., 2025). Arabic gum, a natural polysaccharide, has excellent water retention properties, film-forming ability, and biocompatibility, making it an ideal component for hydrogel-based adsorbents. Additionally, Arabic gum contains hydroxyl and carboxyl groups, which facilitate electrostatic interactions with pollutants, enhancing adsorption efficiency(Verma et al., 2026b). In addition, emerging research has focused on tailoring hydrogel networks through advanced synthesis techniques to improve performance and sustainability. Functionalized polymeric systems and hybrid materials have shown promising results in enhancing adsorption kinetics, selectivity, and regeneration capability (Zhao et al., 2025).

Moreover, recent developments in coordination polymers and hybrid frameworks highlight the importance of designing multifunctional materials with controlled architecture and improved physicochemical properties for environmental remediation (Huang et al., 2026).

Pectin, another natural polysaccharide, is abundant in plant cell walls and is commonly used in hydrogel synthesis due to its high gel-forming ability, hydrophilicity, and functional groups that enhance dye adsorption (Biswal, 2024; Koshy et al., 2026). Pectin-based hydrogels exhibit excellent adsorption capacity, swelling behavior, and chemical stability, making them promising materials for water purification (Koshy et al., 2026; Martínez-Sabando et al., 2023; Mashhadi et al., 2026). By combining Arabic gum and pectin, a biopolymer-based hydrogel network can be designed with enhanced mechanical strength, water absorption, and adsorption efficiency for wastewater treatment (Al-Gethami et al., 2024).

Furthermore, the incorporation of metal oxide nanoparticles into hydrogel matrices has been demonstrated to significantly enhance adsorption capacity, surface reactivity, and multifunctional properties such as antimicrobial activity (Sayed et al., 2025c). Recent studies have reported the development of advanced nanocomposite hydrogels with improved adsorption efficiency and structural stability for water purification applications (Yang et al., 2025; Zhang et al., 2025a). Metal-oxide adsorbents have been set using various techniques that give large yields, high photocatalytic action, an enviable dynamic surface area, little toxicity, and little economical charge. Taking into consideration that metal-oxides acquire double assets: they are used in biotic wastewater treatment for disinfection and chemical waste-water treatment for adsorption (Eldondaity et al., 2026).

Crosslinked hydrogels exhibit high adsorption efficiency due to their remarkable water uptake capacity without dissolution, which enhances the available surface area and facilitates multiple adsorption mechanisms, including ion exchange, chemisorption, hydrogen bonding, complexation, and electrostatic interactions (Alkhaldi et al., 2026). Hydrogels based on grafted polysaccharides such as starch, cellulose, and natural gums with Diethylaminoethyl Methacrylate (DEAEMA) have gained attention for dye wastewater treatment due to their low cost, biodegradability, reusability, and operational simplicity (Taktak & Şimşek, 2022). DEAEMA, an ester of methacrylic acid, is a hydrophobic monofunctional monomer with a low glass transition temperature, making it suitable as a flexible and plasticizing component in polymer networks (Othman et al., 2020). It readily forms homo- and copolymers and undergoes

addition reactions with various compounds, enhancing its versatility in functional material design (Zhang et al., 2025a). Despite recent advancements, several challenges persist, including reliance on toxic chemical initiators, limited control over crosslinking architecture, and inadequate mechanical stability and reusability of adsorbents (Verma et al., 2026b). In addition, many reported systems do not fully achieve a green synthesis route or effectively integrate biopolymer sustainability with nanocomposite functionality (Zhang et al., 2025b).

In this context, gamma irradiation–induced polymerization has emerged as an eco-friendly and efficient alternative, enabling simultaneous grafting and crosslinking without the need for chemical initiators (Mahmoud et al., 2019). This approach provides better control over network formation, enhances material purity, and improves mechanical strength and swelling behavior (Khozemy et al., 2018). Moreover, the in situ generation of free radicals ensures uniform crosslinking while minimizing environmental and health risks associated with conventional methods (Metwally et al., 2026).

In this study, pectin/Arabic gum-g-DEAEMA hydrogels and CuO-incorporated nanocomposite hydrogels are synthesized via gamma irradiation–induced copolymerization and crosslinking, offering a clean, initiator-free route that ensures uniform network formation, enhanced structural integrity, and improved material purity. The incorporation of CuO nanoparticles further enhances adsorption efficiency, thermal stability, and antimicrobial functionality.

The novelty of this work lies in the integration of a fully green irradiation driven synthesis with a biopolymer, based hydrogel system and CuO nanostructures within a single platform, enabling simultaneous improvement in adsorption performance and multifunctional properties.

Compared to conventional approaches, the developed hydrogels exhibit a synergistic combination of green synthesis, controlled crosslinking, and high adsorption efficiency, making them promising candidates for sustainable methylene blue removal from wastewater. Comprehensive characterization establishes clear structure–property–performance relationships, highlighting their potential for advanced environmental remediation applications.

2 Materials and Methods

2.1 Materials

Sigma-Aldrich (China) supplied apple peel-isolated pectin powder (PC) with 50–75% esterification. German Aldrich supplied 99.9% pure 2(Dimethylamino) ethyl methacrylate (DMAEMA), while Sigma-Aldrich USA sourced-Arabic gum. Other chemicals were sourced from El-Nasr Co. and used without further purification.

2.2 Preparation of Pectin/Arabic Gum/DMAEMA Hydrogel

The Pectin/Arabic gum/DMAEMA solution dissolved 2 g of pectin and 2 g of Arabic gum in 70 mL distilled water at 80 °C for 30 min. After an hour of mixing and stirring at room temperature, 30 mL of DMAEMA was added and mixed for another hour to create a homogenous solution mixture of a total polymer/monomer concentration of 34 wt%. The solution was placed in a glass tube and subjected to γ-ray irradiation from a Co-60 source at a dose of 20 kGy. The necessary irradiation dosage was achieved in the cobalt-60 gamma cell (Canada) at a dose rate of 0.98 kGy/h in air. This source was deployed for study at the NCRRT at Egypt's Atomic Energy Authority. Hydrogels were obtained as rods, which were then sliced into smaller pieces. After drying in air to a constant weight, all samples were submerged in distilled water for 24 h at 70 °C to remove the unreacted component.

2.3 Preparation of CuO@ Pectin/Arabic Gum/DMAEMA Hydrogel Nanocomposite

A known dry weight of Pectin/Arabic gum/DMAEMA hydrogel was put in 1.0 mol/L $CuSO_4$ solution for 12 h. Loaded samples were immersed in distilled water for 24 h to remove unbound and physically bonded metal ions. After that, they were shaken overnight in 0.5 mol/L NaOH in a water shaker bath at room temperature. To ensure reduction, three drops of glycerol were added. The CuO@ Pectin/Arabic gum/DMAEMA nanocomposites were submerged in distilled water for 12 h and then dried in a 40 °C oven (Scheme 1).

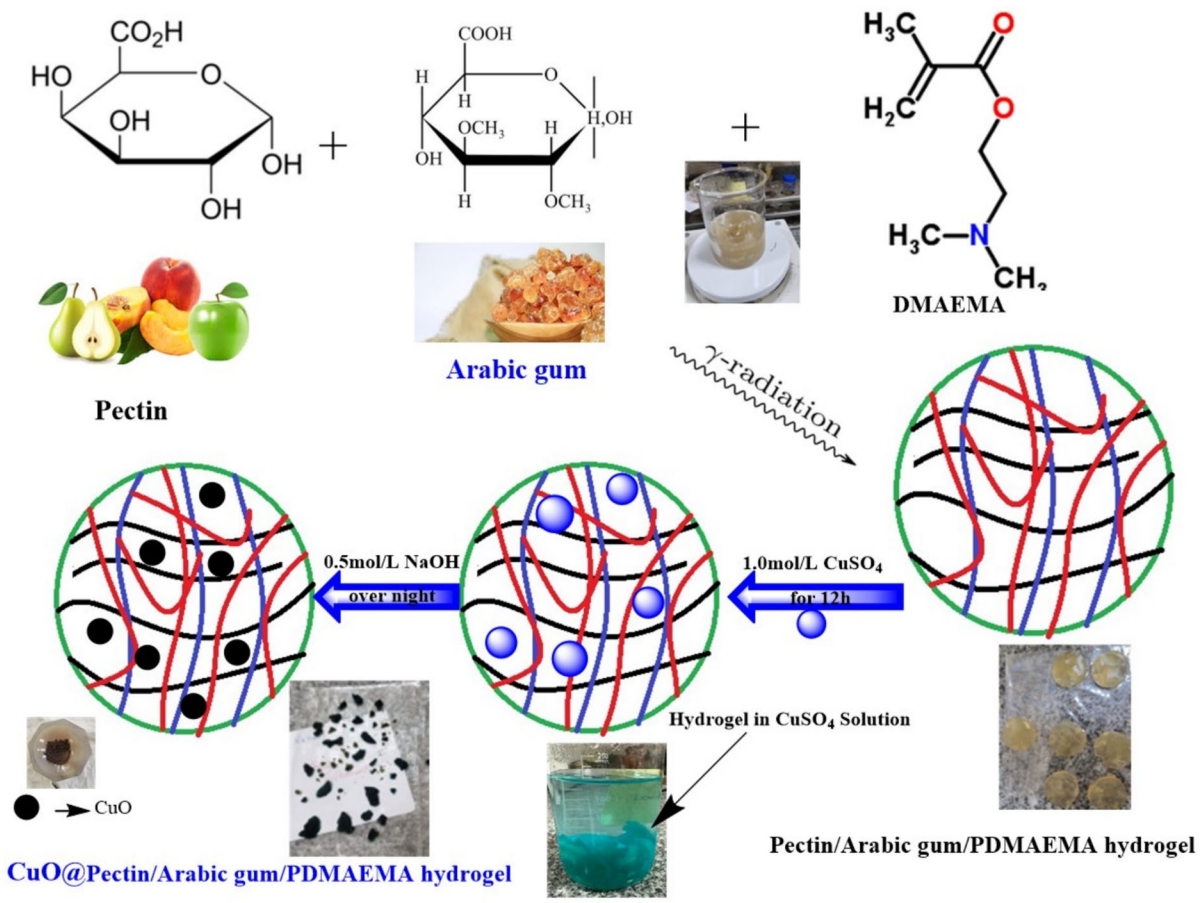

Scheme 1 Preparation steps of Pectin/Arabic gum/DMAEMA hydrogel and CuO@ Pectin/Arabic gum/PDMAEMA nanocomposites

2.4 Instrumentation and Characterization

2.4.1 Particle Size and Zeta Potential Measurements

The particle size and zeta potential CuO nanoparticles are determined using a dynamic light scattering instrument (ZetaSizer Nano Series (HT), Nano ZS, Malvern Instruments London, England) at 25 °C.

2.4.2 X-Ray Diffraction Analysis

A Shimadzu XDDI Series device equipped with a copper target (wavelength (λ) = 1.542 Å) was used for X-ray diffraction (XRD) analysis. The device operated at an electric current of 30 mA and a voltage of 40 kV. The scanning angle (2θ) ranged from 4° to 90° at a scanning speed of 8°/min.

2.4.3 Energy Dispersive X-Ray Analysis (EDX)

The elemental composition of the CuO nanoparticles was determined using an energy-dispersive X-ray (EDX) unit (EDX; Zeiss-LEO-438VP, Oxford Instrumentations with INCA software) applied to investigate the chemical composition at a 20 kV acceleration voltage and a 21 mm operational distance.

2.4.4 Fourier Transform Infrared Spectroscopy (FT-IR)

The infrared spectra of the prepared hydrogels were obtained using an FT-IR model Bruker, Unicom infrared spectrophotometer, Germany, and were recorded at a wavelength range of 400–4000 cm^{-1}.

2.4.5 Thermogravimetric Analysis (TGA)

Thermogravimetric analysis (TGA) was performed at a heating rate of 10 °C/min in a nitrogen atmosphere using a Shimadzu TGA-30 (Japan).

2.4.6 Scanning Electron Microscopy (SEM) Analysis

The surface morphology of the prepared nanocomposite was analyzed using a high-resolution scanning electron microscope (SEM) equipped with a ZEISS LEO 1530 Gemini Optics Lens. The microscope operated at an accelerated voltage of 30 kV, allowing for detailed imaging of the nanoparticle surfaces.

2.4.7 Brunauer–Emmett–Teller (BET)

BET surface area analysis was performed using a BELSORP-MAX instrument based on nitrogen adsorption–desorption isotherms measured at 77.35 K. Prior to analysis, the samples were degassed at 120 °C for 24 h under vacuum up to 10^{-2} bar to remove physically adsorbed moisture and activate the surface. The total pore volume was estimated from the adsorption isotherm at a relative pressure of $P/P_0 = 0.995$, assuming complete pore saturation.

2.5 Swelling Properties

A known weight of sample W_d was submerged in 50 mL of distilled water until equilibrium was established. The swollen sample was reweighed W_s after filter paper dried the surface water. The swelling process was tested at different pH levels. Calculating swelling % utilized this equation:

$$\text{Equilibrium swelling}\,(\%) = \frac{W_s - W_d}{W_d} \times 100 \qquad (1)$$

2.6 Adsorption Study

A 50 mL known starting concentration of MB solution at pH 3 was added to 0.1 g of dry adsorbent and stirred for a defined time. This equation calculated MB dye removal.

$$\text{MB dye Removal}\,(\%) = \frac{(C_o - C_e)}{C_o} \times 100 \qquad (2)$$

C_0 and C_e are the initial and final concentrations in mg/L. The MB dye concentration was measured using a Jasco model V-530 UV/VIS spectrometer with a 1.0 cm quartz cell at wavelength nm.

2.7 Antimicrobial Analysis

The antimicrobial properties of both pectin/Arabic gum-g-PDMAEMA hydrogel and CuO@pectin/Arabic gum-g-PDMAEMA nanocomposite hydrogel were investigated against two fungal strains, *Candida albicans (ATCC 10231) (CA) and Aspergillusniger (ATCC) (ASP*), as well as four bacterial species: the Gram-positive bacteria *Staphylococcus aureus (ATCC 29213)* (SA) and *Bacillus subtilis (ATCC 6051)* (BS), and the Gram-negative bacteria *Klebsiella pneumoniae (ATCC 700603)* (KP) and *Escherichia coli (ATCC 25922)* (EC). The disc diffusion method was used to evaluate the antimicrobial activity, and the inhibition zones around the discs were measured.

3 Results and Discussions

The present study aims to prepare a green construction composed of pectin, Arabic gum, and DEAEMA (diethylaminoethyl methacrylate) via gamma irradiation as a green method. CuO nanoparticles were incorporated in situ in the matrix to form a CuO@pectin/Arabic gum/DEAEMA nanocomposite hydrogel to be used as an adsorbent to remove methylene blue (MB) dye. Initially, the CuO nanoparticles will be characterized using Dynamic Light Scattering (DLS) and Energy Dispersive X-ray (EDX) analysis. The pectin/Arabic gum/DEAEMA hydrogel and the CuO@pectin/Arabic gum/DEAEMA nanocomposite hydrogel were characterized through Fourier Transform Infrared Spectroscopy (FTIR), Thermogravimetric Analysis (TGA), and X-ray Diffraction (XRD). The hydrogel's and the nanocomposite hydrogel's swelling properties and antibacterial activity were evaluated. A morphological study was also conducted using Field Emission Scanning Electron Microscopy (FESEM) before and after MB dye loading. Finally,

the adsorption of MB dye was studied as a function of the dye solution pH, adsorbent weight (g), contact time, and MB dye concentration.

3.1 Characterization of CuO Nanoparticles

The successful synthesis of copper oxide (CuO) nanoparticles was confirmed through a series of characterization techniques, each providing critical insights into the nanoparticles' structural, compositional, and physical properties (Fig. 1).

The Dynamic Light Scattering (DLS) analysis revealed that the synthesized CuO nanoparticles possess an average particle size of approximately 47 nm (Fig. 1a). This nanoscale dimension is particularly advantageous for applications in hydrogel matrices, as it offers a higher surface area-to-volume ratio. Such a ratio enhances the interactions between the nanoparticles and the hydrogel components, thereby improving the efficiency of methylene blue (MB) dye adsorption. As indicated by the narrow peak in the DLS data, the uniformity in particle size distribution suggests a consistent and reproducible synthesis process, which is essential for achieving reliable performance in practical applications. Precise control over nanoparticle size distribution is crucial, as it directly influences the kinetics and capacity of dye removal when integrated into the hydrogel network.

The X-ray Diffraction (XRD) analysis further confirmed the successful synthesis of CuO nanoparticles by identifying distinct diffraction peaks corresponding to CuO's monoclinic crystal phase (Fig. 1b). The prominent peaks observed at 2θ values of 32.5°, 35.5°, 38.7°, 48.7°, and 58.4° are attributed to the (110), (002), (111), (200), and (202) crystal planes, respectively. These diffraction patterns align closely with the standard JCPDS card number 45–0937, indicating the purity of the synthesized CuO nanoparticles. The sharpness and intensity of these peaks reflect a high degree of crystallinity,

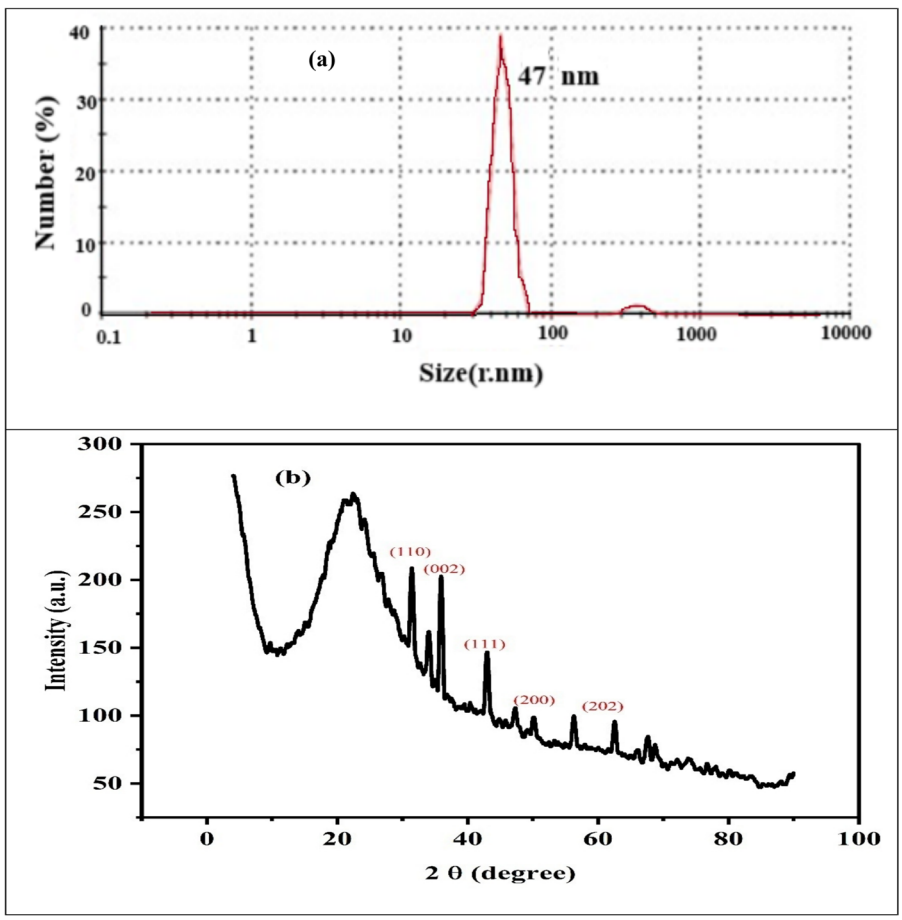

Fig. 1 DLS (a), XRD (b), and EDX (c) analyses of CuO nanoparticles

Fig. 1 (continued)

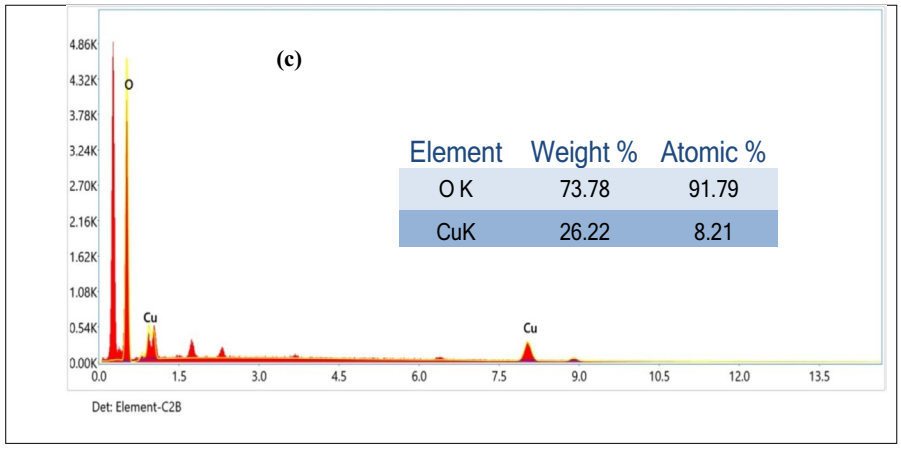

which is often associated with enhanced stability and activity of nanoparticles. Using the Debye–Scherrer equation, the crystallite sizes were estimated to range from 36 to 61 nm, with specific measurements showing 45.4 nm at 32.5°, 36.3 nm at 35.5°, and 60.7 nm at 38.7°. These sizes agree with the average particle size determined by DLS, reinforcing the reliability of the synthesis method and confirming that the nanoparticles are free from significant agglomeration. The slight variations in crystallite size across different planes suggest anisotropic growth, which can be beneficial in tailoring specific properties for targeted applications.

The elemental composition of the CuO nanoparticles was examined through Energy Dispersive X-ray (EDX) analysis, providing a quantitative confirmation of their chemical purity (Fig. 1c). The EDX spectrum revealed prominent peaks corresponding to copper (Cu) and oxygen (O), with weight percentages of 26.22% and 73.78%, respectively. The atomic percentages were calculated as 8.21% for Cu and 91.79% for O, supporting the stoichiometric formation of CuO with minimal impurities. This elemental analysis confirms a successful synthesis of CuO nanoparticles, ensuring they possess the desired composition for effective integration into the hydrogel matrix. The presence of minimal impurities is crucial, as it guarantees the consistency and effectiveness of the nanoparticles in enhancing the properties of the CuO@pectin/Arabic gum/DEAEMA nanocomposite hydrogel. This purity is particularly significant for the nanoparticles' role in dye adsorption, as any impurities could interfere with the hydrogel's interaction with methylene blue dye molecules.

The consistent particle size observed in DLS and the crystallite size from XRD confirms a high control over the synthesis process, resulting in well-defined and uniform nanoparticles. This uniformity is critical for the reproducibility and scalability of the nanocomposite hydrogel in real world wastewater treatment scenarios. Furthermore, the elemental purity demonstrated by EDX analysis underscores the reliability of the synthesis method, ensuring that the CuO nanoparticles are performed optimally in the hydrogel matrix to remove methylene blue dye. Collectively, these analyses validate the CuO nanoparticles' potential to enhance the adsorptive properties of the hydrogel, providing a promising, sustainable solution for mitigating water pollution from textile dyes.

3.2 Characterization of CuO@Pectin/Arabic Gum-g-DEAEMA Nanocomposite Hydrogel

CuO@pectin/Arabic gum-g-DEAEMA nanocomposite hydrogel was characterized compared with pectin/Arabic gum-g-DEAEMA hydrogel to elucidate their structural, thermal, and functional properties. This analysis employed several advanced techniques, including FTIR, XRD, and TGA, and provided valuable insights into the interactions between the components.

3.2.1 Fourier Transform Infrared FTIR Analysis

Figure 2a illustrates the FTIR spectra of the pectin/Arabic gum-g-DEAEMA and the CuO@pectin/Arabic gum-g-DEAEMA nanocomposite hydrogel. The FTIR spectrum of the pristine biohydrogel

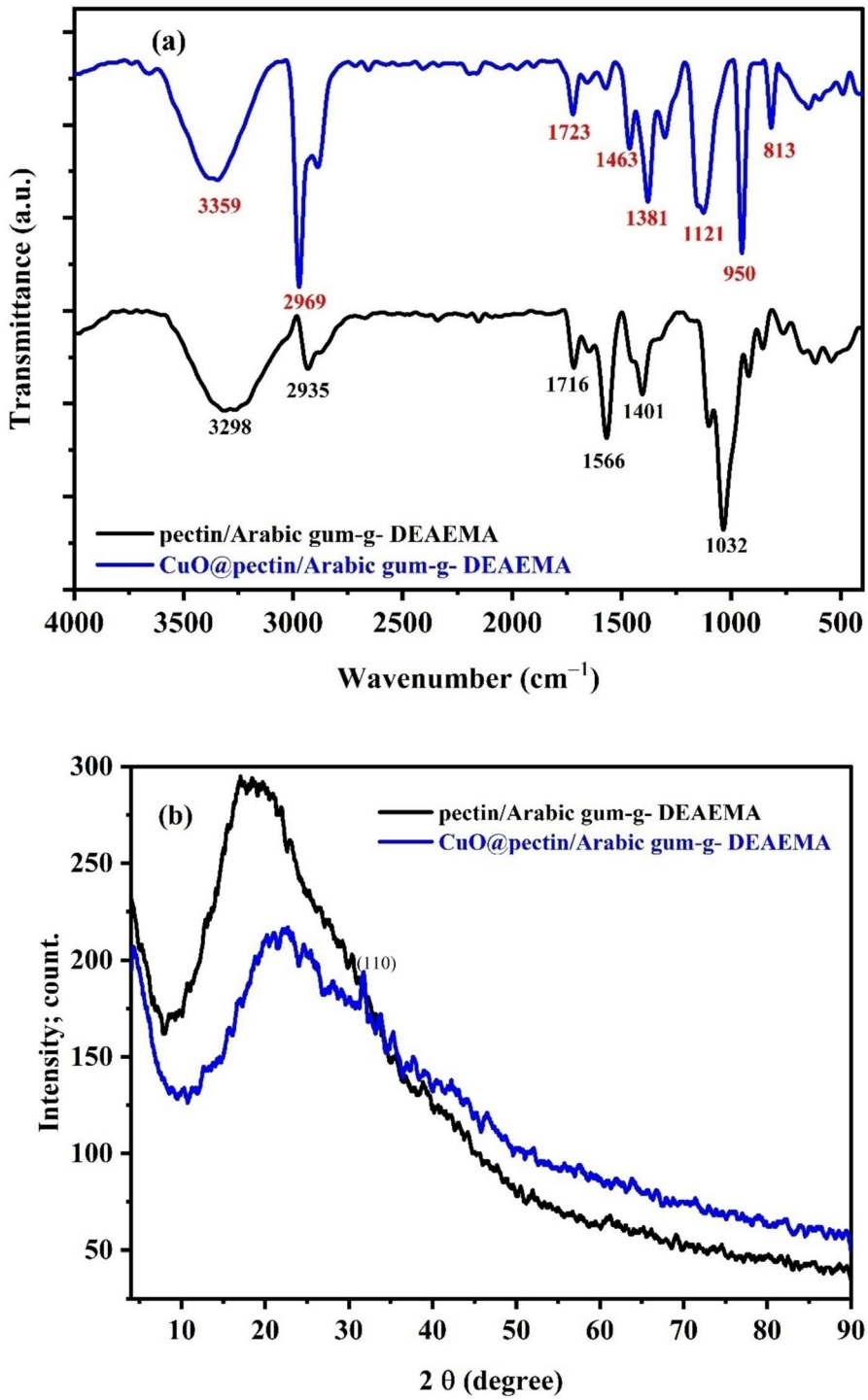

Fig. 2 FTIR analysis (a), XRD (b), TGA (c), DTG (d), and swelling (%) as a function of time (e) of pectin/Arabic gum-g-DEAEMA and CuO@pectin/Arabic gum-g-DEAEMA nanocomposite hydrogels

reveals characteristic absorption bands, with a broad peak around 3410 cm^{-1}, corresponding to the O–H stretching vibrations of hydroxyl groups (Nezhad-Mokhtari et al., 2024)present in pectin and Arabic gum. Peaks at 2920 cm^{-1} and 2850 cm^{-1} indicate C-H stretching vibrations, while the band at 1725 cm^{-1} is attributed to the C = O stretching of the carbonyl group (Mohamed et al., 2023; Yadav & Yadav,

Fig. 2 (continued)

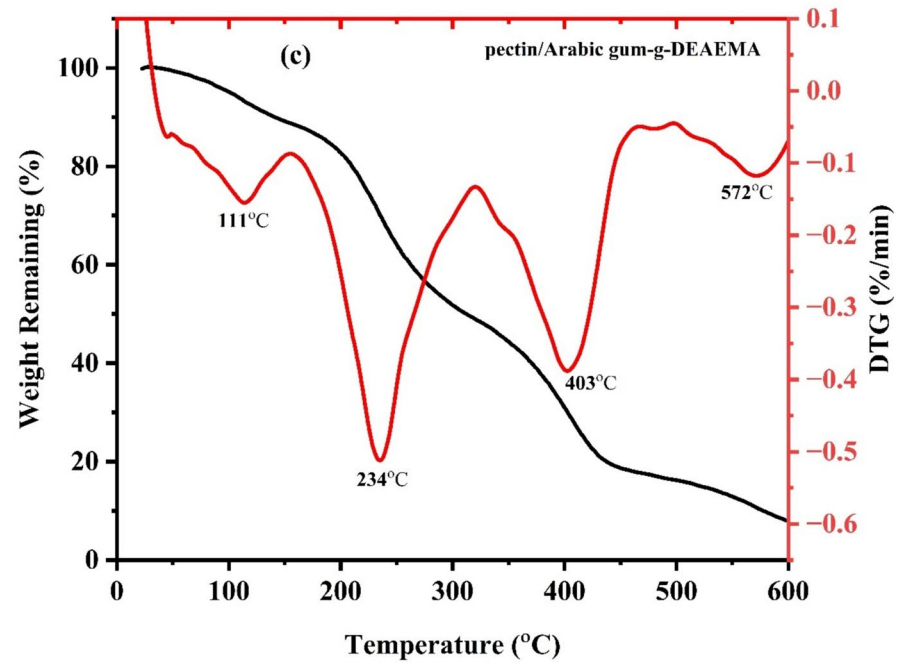

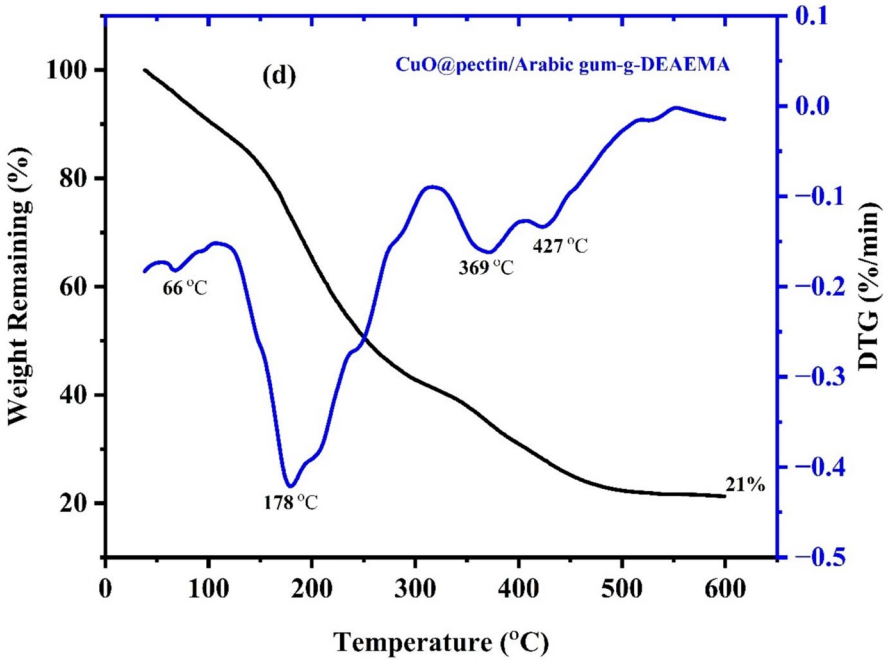

2005). A prominent band at 1450 cm^{-1} reflects C-N stretching vibrations, confirming the incorporation of DEAEMA into the hydrogel network (Hamze et al., 2024; Levien et al., 2023). In the CuO@pectin/Arabic gum-g-DEAEMA nanocomposite hydrogel, the FTIR spectrum retains these key features, suggesting that the structural framework of the polymer matrix remains intact (Ellis & Martin, 2016). However, additional peaks at 530 cm^{-1} and 610 cm^{-1} are observed, corresponding to Cu–O stretching vibrations(Sahai

Fig. 2 (continued)

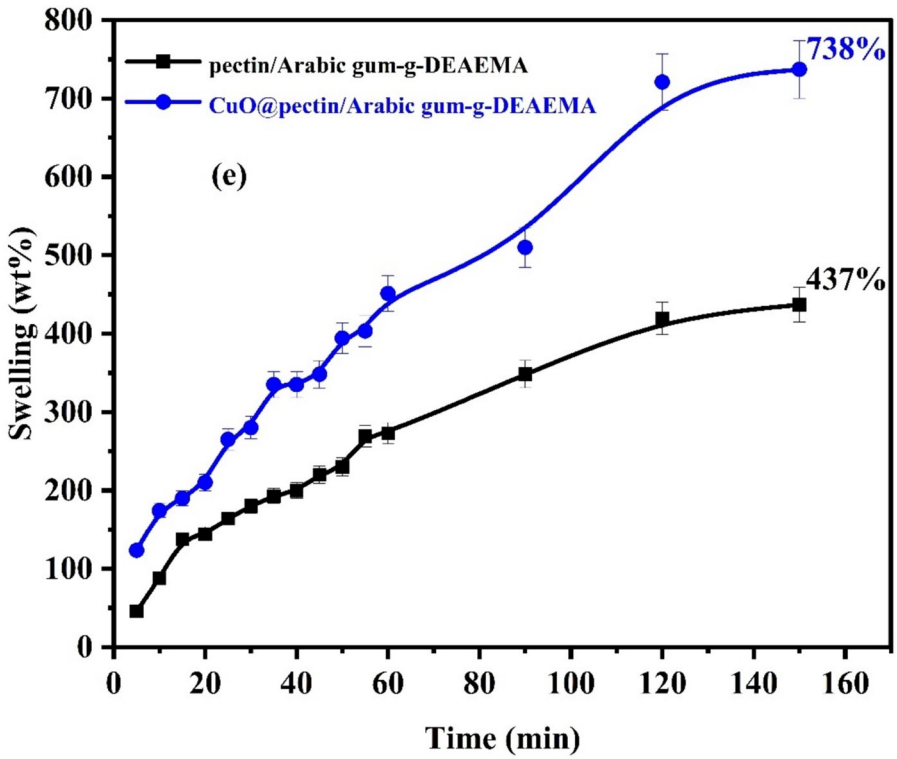

et al., 2018). These bands confirm the successful integration of CuO nanoparticles into the hydrogel matrix, indicating potential interaction sites for pollutant adsorption and providing structural reinforcement to the polymer network.

3.2.2 X-Ray Diffraction XRD Analysis

Figure 2b presents the pectin/Arabic gum-g-DEAEMA XRD patterns and the CuO@pectin/Arabic gum-g-DEAEMA nanocomposite hydrogel. The XRD pattern of the pectin/Arabic gum-g-DEAEMA biohydrogel reveals a broad diffraction peak around 2θ 21°, indicative of its amorphous nature. This amorphous structure is characteristic of hydrogels, providing flexibility and swelling capability beneficial for adsorption applications (Sayed et al., 2022a). The XRD pattern of the CuO@pectin/Arabic gum-g-DEAEMA nanocomposite hydrogel shows distinct diffraction peaks at 2θ value of 32.4°corresponding to the crystalline plane (110) of CuO nanoparticles. The presence of this peak confirms the successful incorporation and crystallinity of CuO within the hydrogel matrix. The CuO nanoparticles enhance the hydrogel's mechanical properties(Krishna et al., 2024; Mallakpour et al., 2020), increasing its robustness (Deo et al., 2019)and making it suitable for various environmental applications where structural integrity is essential(Shang et al., 2021).

3.2.3 Thermogravimetric Analysis TGA Analysis

TGA and derivative thermogravimetric (DTG) thermograms of the pectin/Arabic gum-g-DEAEMA hydrogel (Fig. 2c) and the CuO@pectin/Arabic gum-g-DEAEMA nanocomposite hydrogel (Fig. 2d) illustrate their thermal stability and decomposition profiles. The TGA curve of the pectin/Arabic gum-g-DEAEMA biohydrogel exhibits multiple degradation steps, with the first weight loss at around 111 °C attributed to moisture evaporation and the removal of loosely bound water. The second major degradation step occurs at approximately 234 °C, corresponding to the breakdown of polysaccharide structures. Further decomposition peaks are observed at 403 °C and 572 °C, indicating the thermal degradation of the grafted polymer chains and residual char oxidation. The CuO@pectin/Arabic

gum-g-DEAEMA nanocomposite hydrogel demonstrates a shift in thermal stability due to the incorporation of CuO nanoparticles. The initial weight loss occurs at a lower temperature (~ 66 °C), suggesting increased water retention within the nanocomposite. The primary degradation peaks are recorded at 178 °C, 369 °C, and 427 °C, with a notable residue of 21% at 600 °C, which is significantly higher than the pristine hydrogel. This residual mass is attributed to the presence of CuO nanoparticles, which enhance thermal stability by acting as a barrier against thermal decomposition. The comparative analysis of these thermograms indicates that the CuO-modified biohydrogel exhibits improved thermal resistance and structural integrity, making it potentially more suitable for applications requiring enhanced stability under elevated temperatures.

Conversely, the CuO-enhanced nanocomposite hydrogel exhibits improved thermal stability, with a delayed onset of major decomposition at around 300°C. This enhancement is attributed to CuO nanoparticles, which act as a reinforcing agent within the hydrogel matrix. The CuO particles not only bolster the structural integrity of the hydrogel but also offer a barrier effect, slowing the thermal degradation of organic components(Oun & Rhim, 2017). Such improved thermal resistance is advantageous for applications requiring durability under thermal stress (Wu et al., 2022).

3.3 Swelling Studies

The swelling percentage of hydrogels is a critical parameter, indicating their capacity to absorb water, which directly influences their adsorption efficiency for pollutants (Sayed et al., 2022b). The swelling behavior of the pectin/Arabic gum-g-DEAEMA biohydrogel and the CuO@pectin/Arabic gum-g-DEAEMA nanocomposite hydrogel over time is illustrated in Fig. 2e. The swelling (%) gradually increased with a high swelling rate for pristine biohydrogel and its nanocomposite. The swelling study reveals that the pristine biohydrogel exhibits a swelling percentage of approximately 437% after three hours of immersion in water, demonstrating good water absorption due to the hydrophilic nature of pectin and Arabic gum. However, the CuO@pectin/Arabic gum-g-DEAEMA nanocomposite hydrogel exhibits a significantly higher swelling percentage of 737%, indicating enhanced water uptake capacity. This increase in swelling is attributed to the CuO nanoparticles, which improve the surface area (Abdollahi et al., 2021) and hydrophilicity (Yadollahi et al., 2015) of the hydrogel. The enhanced swelling capability facilitates greater interaction between the hydrogel matrix and pollutant molecules, such as methylene blue dye, leading to improving the adsorption performance (Gao et al., 2021; Sun et al., 2023). The ability to swell more extensively makes the CuO-loaded hydrogel particularly suitable for applications in dye removal from wastewater, where efficient pollutant interaction is required (Rahman & Rimu, 2022).

3.4 BET Surface Area and Porosity Analysis

Nitrogen adsorption–desorption analysis was performed to evaluate the surface area and porous structure of the pectin/Arabic gum-g-DEAEMA biohydrogel and the CuO@pectin/Arabic gum-g-DEAEMA nanocomposite hydrogel, as shown in Fig. 3a and b. The obtained BET and porosity parameters are summarized in Table 1.

The pectin/Arabic gum-g-DEAEMA biohydrogel exhibited a BET surface area of 14.05 $m^2\ g^{-1}$, a total pore volume of 0.08685 $cm^3\ g^{-1}$, and a mean pore diameter of 24.728 nm. These values indicate that the pectin/Arabic gum-g-DEAEMA biohydrogel possesses a mesoporous structure, which is favorable for methylene blue adsorption because it facilitates dye diffusion into the hydrogel network and improves the accessibility of active functional groups such as hydroxyl, carboxyl, and amine groups (Sayed et al., 2025b).

After CuO incorporation, the BET surface area increased to 28.22 $m^2\ g^{-1}$, while the total pore volume increased to 0.2201 $cm^3\ g^{-1}$ and the mean pore diameter reached 31.203 nm. This enhancement confirms that CuO nanoparticles contributed to the development of a more open and accessible porous structure. The improvement may be attributed to the dispersion of CuO nanoparticles within the hydrogel matrix, which increases surface roughness, creates additional adsorption-active sites, and improves mass transfer pathways (Sayed et al., 2026).

The adsorption–desorption isotherms of both samples exhibit features typical of mesoporous materials, with increased nitrogen uptake at higher relative pressure, indicating capillary condensation within mesopores. The NLDFT pore-size distribution curves

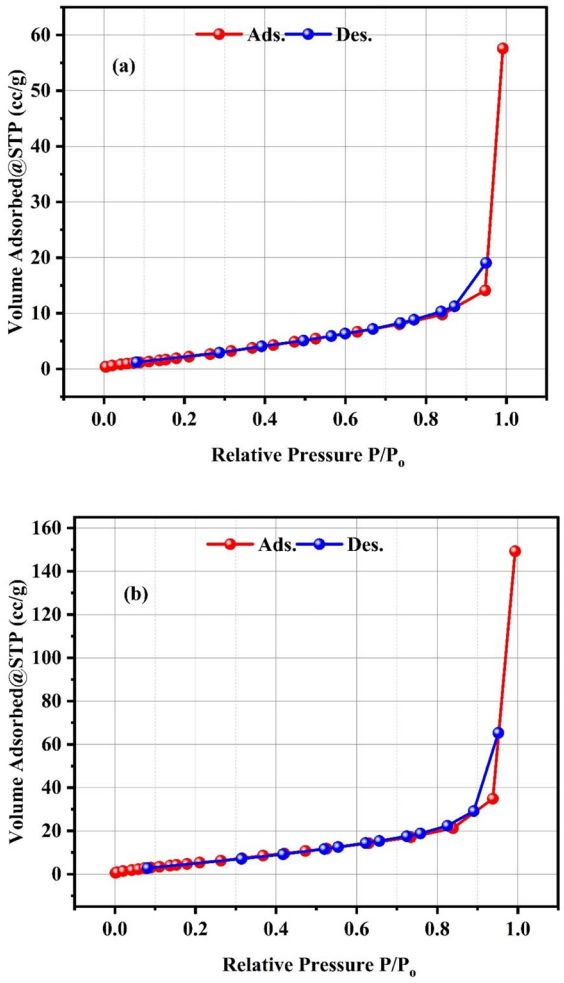

Fig. 3 Nitrogen adsorption–desorption isotherms of (a) pectin/Arabic gum-g-DEAEMA biohydrogel and (b) CuO@pectin/Arabic gum-g-DEAEMA nanocomposite hydrogel, and (c) NLDFT pore-size distribution curves

in Fig. 3c further confirmed the mesoporous nature of both materials. The pectin/Arabic gum-g-DEAEMA biohydrogel showed a narrow pore-size distribution centered at approximately 15.6 nm, while the CuO@pectin/Arabic gum-g-DEAEMA nanocomposite hydrogel displayed a distribution centered at approximately 22.8 nm. This shift toward larger pores after CuO incorporation supports the formation of a more developed mesoporous network.

So, the increase in surface area, pore volume, and pore size after CuO incorporation plays an important role in enhancing methylene blue adsorption by improving dye diffusion and increasing the accessibility of active adsorption sites. These findings confirm that the CuO-loaded nanocomposite hydrogel has more favorable textural properties for efficient wastewater remediation applications.

3.5 Antimicrobial Activity

Figure 4 highlights the antimicrobial activity of the pectin/Arabic gum-g-DEAEMA biohydrogel and the CuO@pectin/Arabic gum-g-DEAEMA nanocomposite hydrogel, emphasizing their potential role in wastewater treatment applications. The presence of microbial contaminants in wastewater significantly affects water quality and the efficiency of dye removal processes. The results demonstrate that incorporating CuO nanoparticles into the biohydrogel enhances its antimicrobial efficacy, which prevents biofouling and microbial proliferation in wastewater treatment systems (Joshi Navare et al., 2020; Uneputty et al., 2022). Among the tested microorganisms, ***Bacillus subtilis***, a common bacterium found in wastewater, exhibited the highest inhibition zone (26 mm) with the CuO@pectin/Arabic gum-g-DEAEMA hydrogel, compared to 16 mm with the pectin/Arabic gum-g-DEAEMA hydrogel and 19 mm with the control antibiotic. Similarly, ***Candida albicans***, a pathogenic fungus frequently present in industrial effluents, showed a larger inhibition zone (27 mm) with the CuO-modified hydrogel than the control antibiotic (25 mm) and the unmodified hydrogel (18 mm), highlighting its strong antifungal properties. These results suggest that the CuO-modified hydrogel can effectively reduce microbial contamination in wastewater treatment systems. For ***Staphylococcus aureus***, a biofilm-forming bacterium that can clog filtration membranes, the pectin/Arabic gum-g-DEAEMA biohydrogel exhibited a weaker inhibition (12 mm). In contrast, the CuO-loaded hydrogel improved antibacterial activity (15 mm), though slightly lower than the control antibiotic (20 mm). ***Escherichia coli*** and ***Klebsiella pneumoniae***, both indicators of fecal contamination in wastewater, followed a similar trend, with inhibition zones of 16 mm and 15 mm, respectively, for the pectin/Arabic gum-g-DEAEMA hydrogel, increasing to 18 mm and 19 mm with CuO incorporation. This enhancement suggests that CuO nanoparticles mitigate microbial risks associated with wastewater treatment. The increased

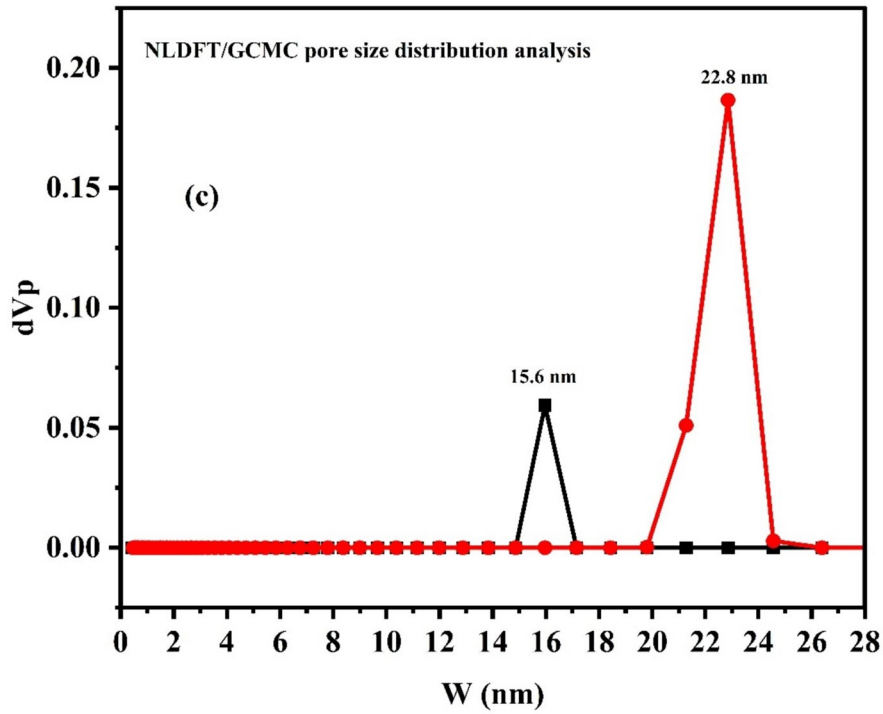

Fig. 3 (continued)

Table 1 BET surface area and porosity parameters of pectin/Arabic gum-g-DEAEMA biohydrogel and CuO@pectin/Arabic gum-g-DEAEMA nanocomposite hydrogel

Sample	(Vm) (cm^3 STP g^{-1})	BET constant, (C)	BET surface area (m^2 g^{-1})	Total pore volume (cm^3 g^{-1})	Mean pore diameter (nm)	NLDFT pore size (nm)
Pectin/Arabic gum-g-DEAEMA biohydrogel	3.2279	4.4795	14.05	0.08685	24.728	15.6
CuO@pectin/Arabic gum-g-DEAEMA nanocomposite hydrogel	6.4836	7.1105	28.22	0.2201	31.203	22.8

antimicrobial efficiency of the CuO@pectin/Arabic gum-g-DEAEMA hydrogel can be attributed to the ability of CuO nanoparticles to generate reactive oxygen species (ROS), which disrupt microbial cell membranes and inhibit their growth (Guan et al., 2021). The hydrogel's strong antibacterial and antifungal effects suggest its potential as a dual-function material for wastewater treatment, both as an adsorbent for dye removal and as an antimicrobial agent to prevent bacterial-induced biofouling (Thapliyal et al., 2025). The results confirm that while the pectin/Arabic gum-g-DEAEMA hydrogel exhibits moderate antimicrobial activity, its effectiveness is significantly enhanced upon CuO nanoparticle incorporation, making it a promising material for sustainable wastewater treatment applications.

3.6 Methylene Blue Removal

3.6.1 Effect of pH

The effect of pH on methylene blue (MB) dye adsorption was investigated for pectin/Arabic gum-g-DEAEMA

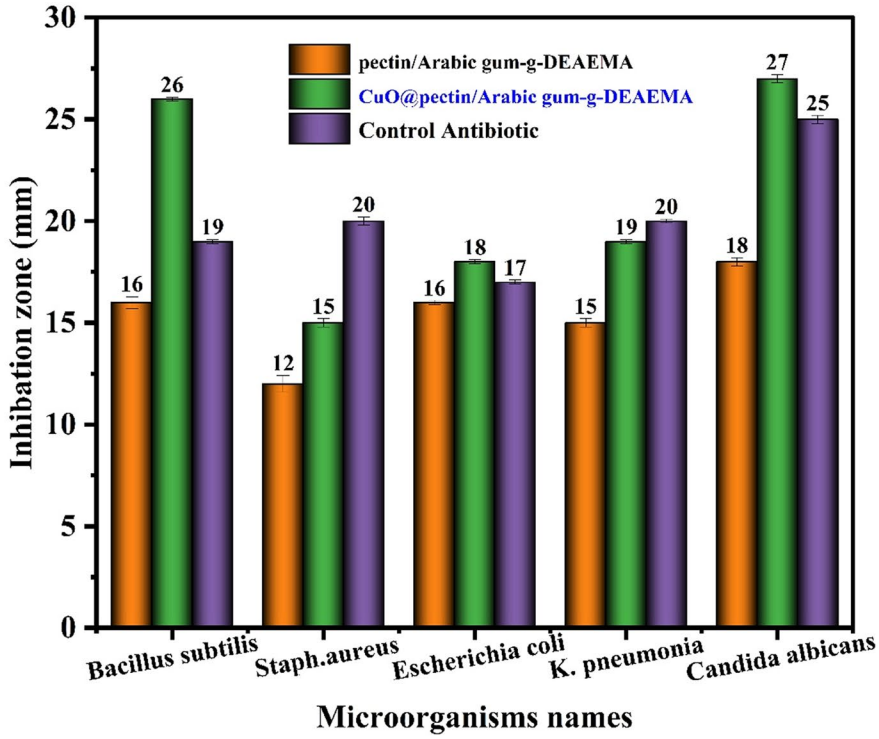
pectin/Arabic gum-g-DEAEMA
CuO@pectin/Arabic gum-g-DEAEMA
Control Antibiotic
Inhibation zone (mm)
0
5
10
15
20
25
30
16
26
19
12
15
20
16
18
17
15
19
20
18
27
25
Bacillus subtilis
Staph.aureus
Escherichia coli
K. pneumonia
Candida albicans
Microorganisms names

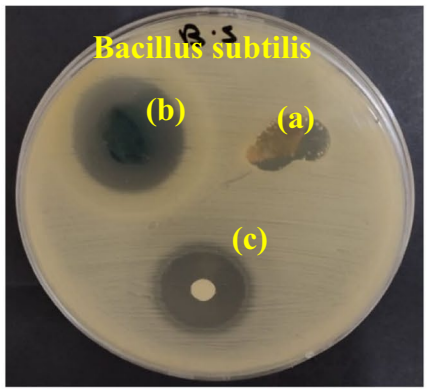
Bacillus subtilis
(a)
(b)
(c)

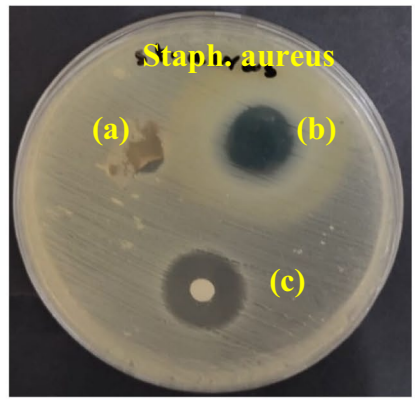
Staph. aureus
(a)
(b)
(c)

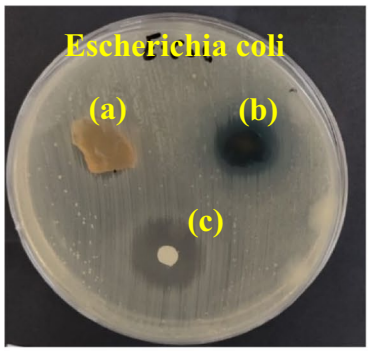
Escherichia coli
(a)
(b)
(c)

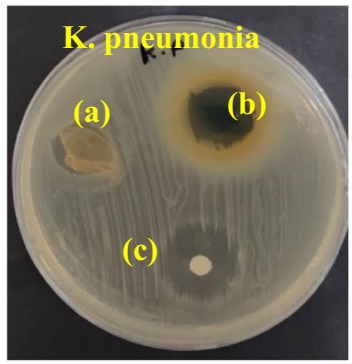
K. pneumonia
(a)
(b)
(c)

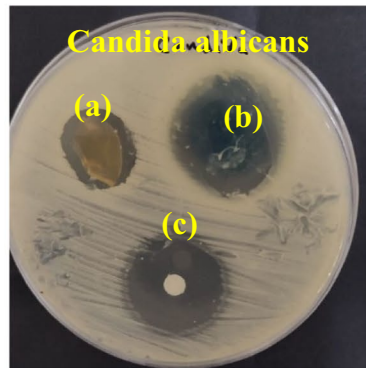
Candida albicans
(a)
(b)
(c)

◂**Fig. 4** Antimicrobial activity of pectin/Arabic gum-g-DEAEMA hydrogel (a) and CuO@pectin/Arabic gum-g-DEAEMA nanocomposite hydrogel (b). Control (c): gentamycin was used for bacteria and fluconazole was used for fungi at a concentration of 1.0 mg/mL

hydrogel and CuO @pectin/Arabic gum-g-DEAEMA nanocomposite. Figure (5a) shows that the highest MB removal was observed at pH 3, with efficiencies reaching approximately 75% for the hydrogel and over 85% for the nanocomposite. Interestingly, a ΔpH versus $pH_{initial}$ plot revealed two zero points of charge (ZPCs) at pH 1.8 and 8.0, indicating amphoteric behaviour of the adsorbent surface due to the coexistence of acidic (e.g., carboxyl from pectin/Arabic gum) and basic (e.g., amine from DEAEMA) functional groups Fig. (5b). Below pH 1.8, the surface is positively charged; above pH 8.0, it becomes negatively charged; between these values, the surface exhibits a near-neutral or mixed charge character. Despite the cationic nature of MB, high removal at pH 3—where the electrostatic attraction is minimal—suggests that non-electrostatic mechanisms govern adsorption. These include hydrophobic interactions between the aromatic dye and the polymer backbone, π–π stacking with electron-rich regions, coordination with CuO nanoparticles, and physical entrapment within the hydrogel matrix, which is enhanced under acidic conditions due to tighter network conformations. This multi-mechanistic adsorption agrees with previous reports emphasizing the role of π–π and hydrophobic interactions in MB uptake onto functionalized polymers and nanocomposites (El-Kousy et al., 2020; Elwakeel, 2009).Thus, the dual-ZPC behaviour and diverse interaction pathways make the CuO@pectin/Arabic gum-g-DEAEMA nanocomposite a promising candidate for effective MB removal, particularly under mildly acidic conditions.

3.6.2 Effect of Bioadsorbent Weight

Figure 5c illustrates the effect of adsorbent weight (g) on the removal percentage of MB dye onto both the pectin/Arabic gum-g-DEAEMA hydrogel and the CuO@pectin/Arabic gum-g-DEAEMA nanocomposite hydrogel at pH 3, with an initial MB dye concentration of 50 mg/L. The results indicate that as the adsorbent weight increases, the removal percentage of MB dye also increases up to 0.75 g. However, no significant increase in removal percentage is observed beyond this weight. This indicates that the system has reached equilibrium, likely due to the saturation of internal adsorption sites and mass transfer limitations that restrict additional MB molecules from accessing unoccupied sites.

3.6.3 Effect of Contact Time

Figure 5d depicts the effect of contact time (min) on the removal percentage of MB dye onto both the pectin/Arabic gum-g-DEAEMA hydrogel and the CuO@pectin/Arabic gum-g-DEAEMAnanocomposite hydrogel at pH 3, with an initial MB dye concentration of 50 mg/L and an adsorbent weight of 0.75 g. The results show that the removal percentage of MB dye increases with contact duration, indicating that adsorption happens quickly in the early phases due to the abundance of active binding sites on the hydrogel surface. As contact time increases, more MB dye molecules diffuse into the hydrogel network and bind to accessible functional groups, gradually increasing removal efficiency. However, after 60 min, the adsorption process reaches equilibrium, and no valuable change in the removal percentage is noted. This equilibrium state may be attributed to the saturation of adsorption sites, where most binding sites are occupied, or mass transfer limitations that restrict additional MB molecules from accessing unoccupied sites. Furthermore, the adsorption and desorption rates may become balanced at equilibrium, avoiding further dye uptake.

3.6.4 Effect of MB Dye Initial Concentration

Figure 5e illustrates the effect of methylene blue (MB) dye initial concentration (mg/L) on the removal percentage of both the pectin/Arabic gum-g-DEAEMA hydrogel and the CuO@pectin/Arabic gum-g-DEAEMA nanocomposite hydrogel at pH 3, with a contact time of 60 min and an adsorbent weight of 0.75 g. The results reveal distinct trends for the two materials: for the CuO@pectin/Arabic gum-g-DEAEMAnanocomposite hydrogel, the removal percentage remains at 100% until an initial dye concentration of 20 mg/L gradually decreases. This decline happens significantly slower than in the pectin/Arabic

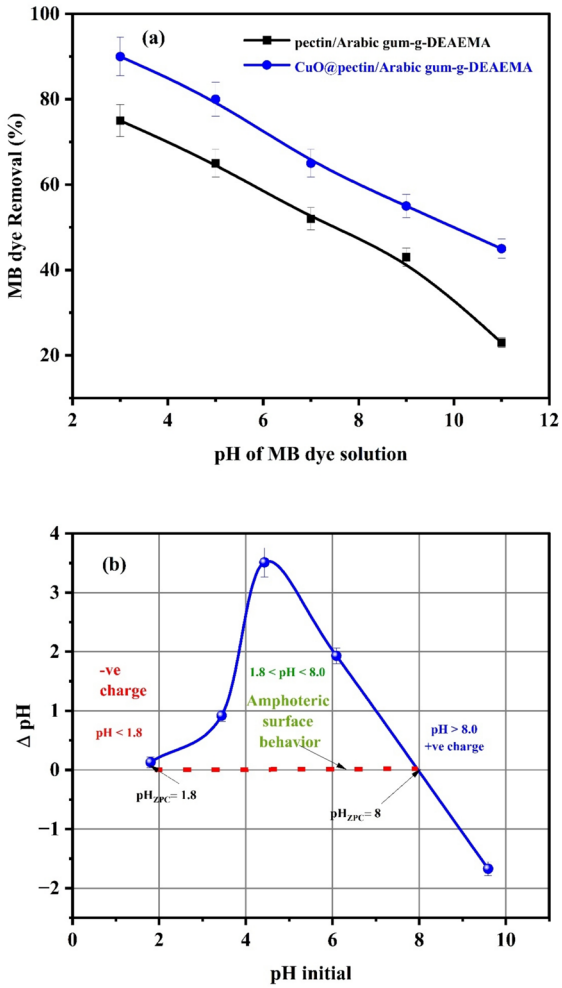

Fig. 5 Effect of pH (a), zero point of charge (b), bioadsorbent weight (c), contact time (d), and initial MB dye concentration (e) on the removal (%) of MB dye using pectin/Arabic gum-g-DEAEMA hydrogel and CuO@pectin/Arabic gum-g-DEAEMA nanocomposite hydrogel, and (f) pictorial illustration of the MB dye adsorption process

Fig. 5 (continued)

gum-g-DEAEMA hydrogel. The CuO@pectin/Arabic gum-g-DEAEMA nanocomposite hydrogel has a higher sustained adsorption capability.

The observed trends highlight the different adsorption behaviors of the two biohydrogels in response to varying initial dye concentrations. The pectin/Arabic gum-g-DEAEMA hydrogel exhibits a decrease in removal percentage with increasing initial dye concentration, indicating saturation of available adsorption sites at higher dye concentrations. In contrast, the CuO@pectin/Arabic gum-g-DEAEMA nanocomposite hydrogel maintains a removal percentage of 100% up to an initial dye concentration of 20 mg/L before gradually decreasing, suggesting a higher adsorption capacity and resilience to higher dye concentrations. The superior performance of the CuO@pectin/Arabic gum-g-DEAEMA nanocomposite hydrogel can be attributed to the presence of CuO nanoparticles, which enhance the adsorption capacity and provide additional active sites for dye molecules. The gradual decrease in removal percentage at higher dye concentrations indicates the eventual saturation of these active sites, albeit at a much slower rate compared to the pectin/Arabic gum-g-DEAEMA hydrogel. These findings underscore the importance of considering initial dye concentrations when designing adsorption processes using hydrogel materials. The CuO@pectin/Arabic

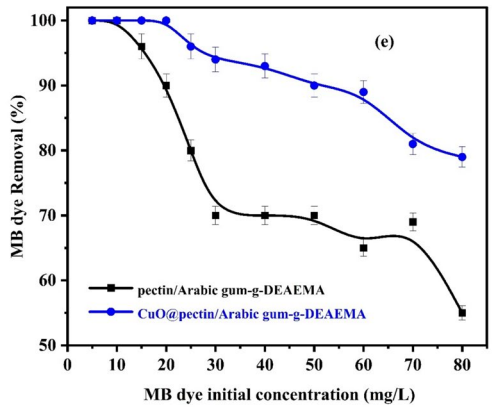

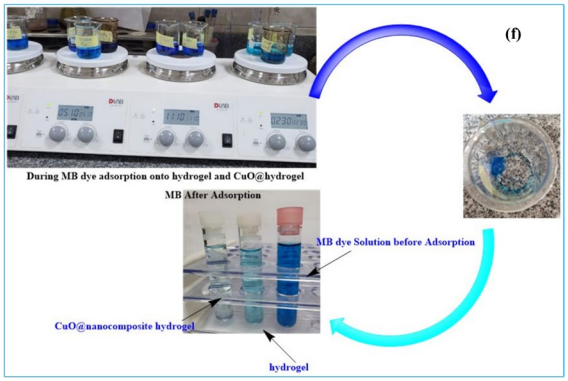

Fig. 5 (continued)

gum-g-DEAEMA nanocomposite hydrogel shows promise for efficient removal of MB dye across a wide range of concentrations, making it a valuable candidate for various water treatment applications.

3.7 Morphological Study

The Morphological study of pectin/Arabic gum-g-DEAEMA hydrogel and CuO@pectin/Arabic gum-g-DEAEMA nanocomposite hydrogel before and after MB dye loaded was investigated by the SEM and presented in Fig. 6.

The SEM image of pectin/Arabic gum-g-DEAEMA hydrogel (Fig. 6a) reveals a highly fibrous and rough surface morphology. For CuO@pectin/Arabic gum-g-DEAEMA nanocomposite hydrogel (Fig. 6b) shows a significantly different surface morphology characterized by compact and crumpled surface morphology. The incorporation of CuO nanoparticles results in a granular appearance, which can enhance the mechanical properties of the hydrogel(Miralaei et al., 2023). The wrinkled surface and distribution of CuO nanoparticles could enhance the available for interactions with external molecules, potentially improving the hydrogel's adsorption capabilities(Qumar et al., 2022).

After MB loading, pectin/Arabic gum-g-DEAEMA hydrogel (Fig. 6c) with a noticeably altered surface. The dye molecules appear to coat the surface uniformly, leading to a smoother appearance. This uniform coating suggests efficient adsorption of MB dye, facilitated by the hydrogel's surface properties rather than pore availability(Wang et al., 2020). The presence of cracks and aggregated structures suggests potential interactions between the dye molecules and the material's surface. For MB dye-loaded CuO@pectin/Arabic gum-g-DEAEMA nanocomposite hydrogel (Fig. 6d), the presence of CuO nanoparticles, which was prominent in the unloaded nanocomposite, is less visible due to the dye coating. The smoother surface indicates that the dye molecules have effectively interacted with and adhered to the hydrogel's surface (Mahmoud et al., 2020). This surface appears more textured, with noticeable deposits and surface irregularities. The increased roughness could indicate dye adsorption onto the composite, potentially through electrostatic interactions or chemical bonding with active sites. This suggests that the nanocomposite's structure allows for substantial dye uptake, which is beneficial for applications requiring effective dye removal.

3.8 Kinetic Study

The adsorption kinetics of methylene blue (MB) dye onto the pectin/Arabic gum-g-DEAEMA and CuO@pectin/Arabic gum-g-DEAEMA nanocomposite hydrogel were evaluated using the pseudo-first-order (PFO) and pseudo-second-order (PSO) kinetic models, as presented in Fig. 7a. The kinetic parameters obtained from fitting the experimental data to these models are summarized in Table 2. The results indicate that both systems follow a PSO kinetic model more closely than the PFO model, as evidenced by the higher R^2 values for PSO in both cases. For pectin/Arabic gum-g-DEAEMA, the PSO

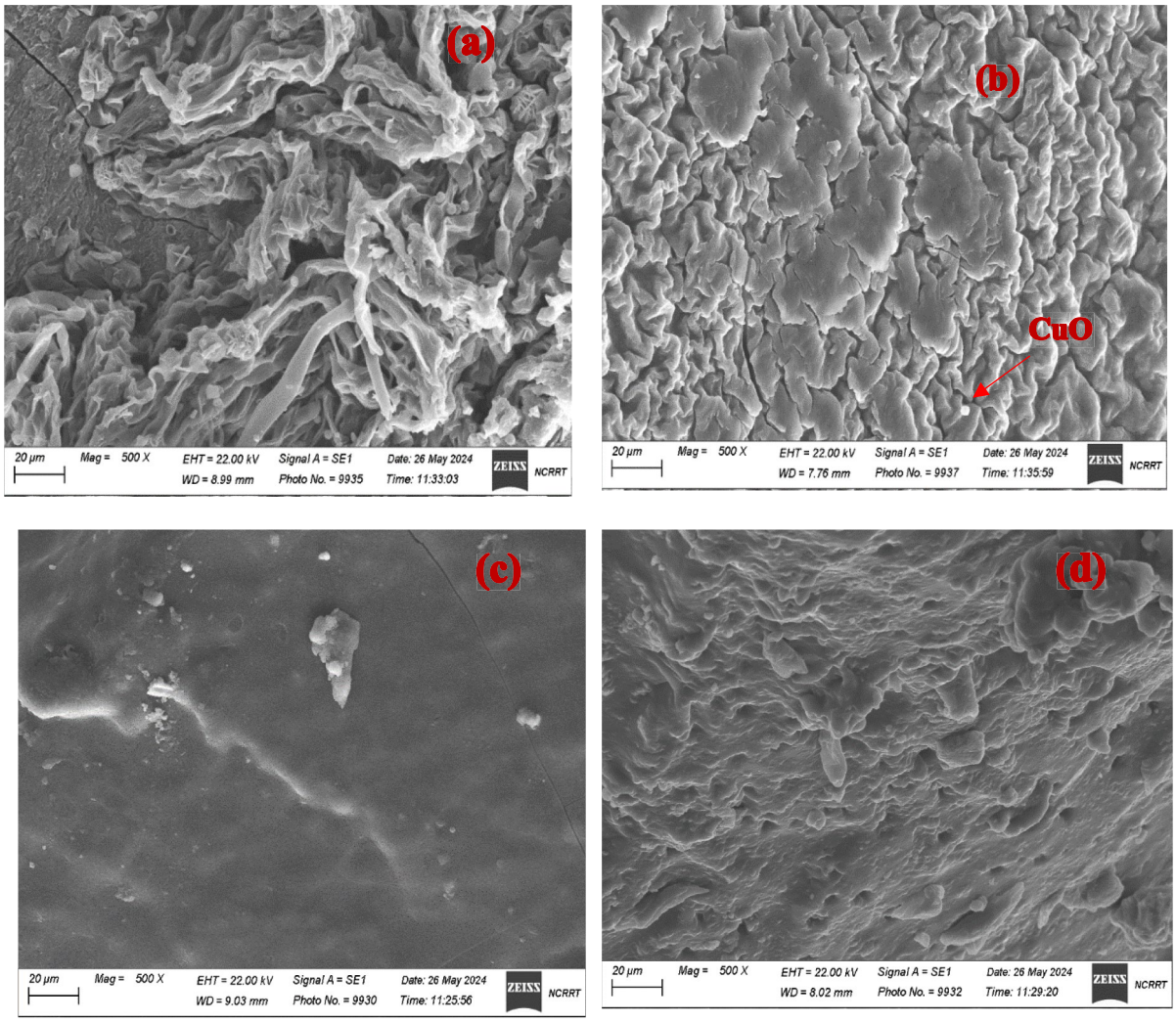

Fig. 6 SEM images of pectin/Arabic gum-g-DEAEMA hydrogel (a), CuO@pectin/Arabic gum-g-DEAEMA nanocomposite hydrogel (b), MB dye-loaded pectin/Arabic gum-g-DEAEMA hydrogel (c), and MB dye-loaded CuO@pectin/Arabic gum-g-DEAEMA nanocomposite hydrogel (d)

model yielded an equilibrium adsorption capacity (qe) of 240.56 mg/g, with a rate constant (k_2) of 1.26515×10^{-4} g/mg·min, achieving a strong correlation coefficient ($R^2 = 0.98912$). In comparison, the PFO model resulted in a lower qe of 207.58 mg/g and a reduced correlation ($R^2 = 0.94752$), suggesting that the chemisorption-based PSO model better describes the adsorption process (Al-Hazmi et al., 2022). Similarly, for CuO@pectin/Arabic gum-g-DEAEMA, the PSO model exhibited a superior fit with an equilibrium adsorption capacity of 256.56 mg/g and a k_2 value of 3.2024×10^{-4} g/mg·min ($R^2 = 0.98529$). The PFO model for the CuO-modified hydrogel resulted in a lower qe of 230.18 mg/g with an improved but still inferior R^2 value of 0.99453, confirming that the PSO model better represents the adsorption process.

The enhancement in qe for the CuO-incorporated hydrogel compared to pectin/Arabic gum-g-DEAEMA hydrogel suggests that CuO nanoparticles contribute to an increased adsorption capacity, likely due to additional active sites and enhanced surface interactions. The faster adsorption kinetics observed in the CuO-modified hydrogel (higher k_2

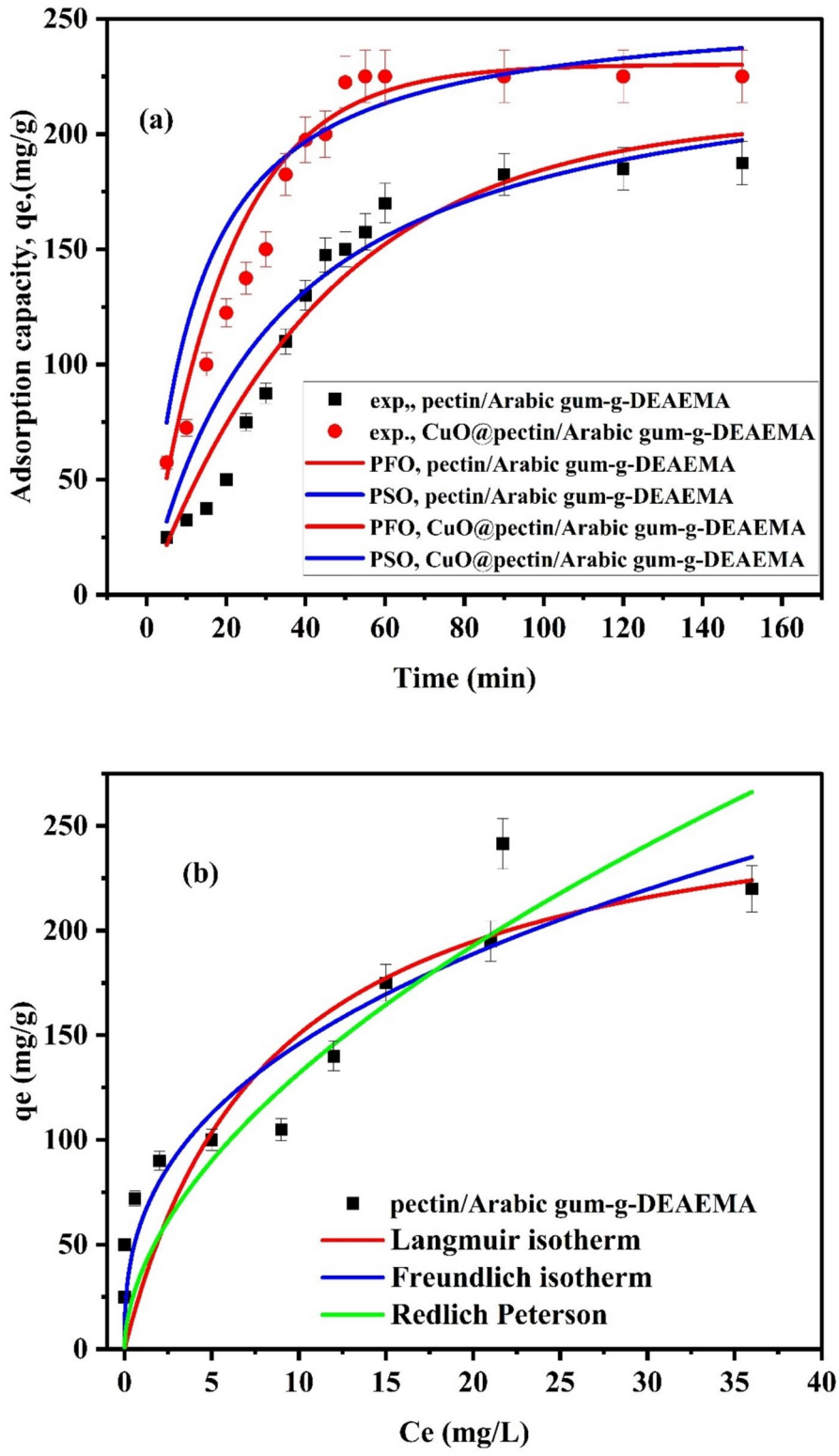

Fig. 7 (a) Adsorption kinetics of MB dye onto pectin/Arabic gum-g-DEAEMA and CuO@pectin/Arabic gum-g-DEAEMA hydrogels; Langmuir, Freundlich, and Redlich–Peterson isotherm models for the adsorption of MB dye onto (b) pectin/Arabic gum-g-DEAEMA hydrogel and (c) CuO@pectin/Arabic gum-g-DEAEMA nanocomposite hydrogel

Fig. 7 (continued)

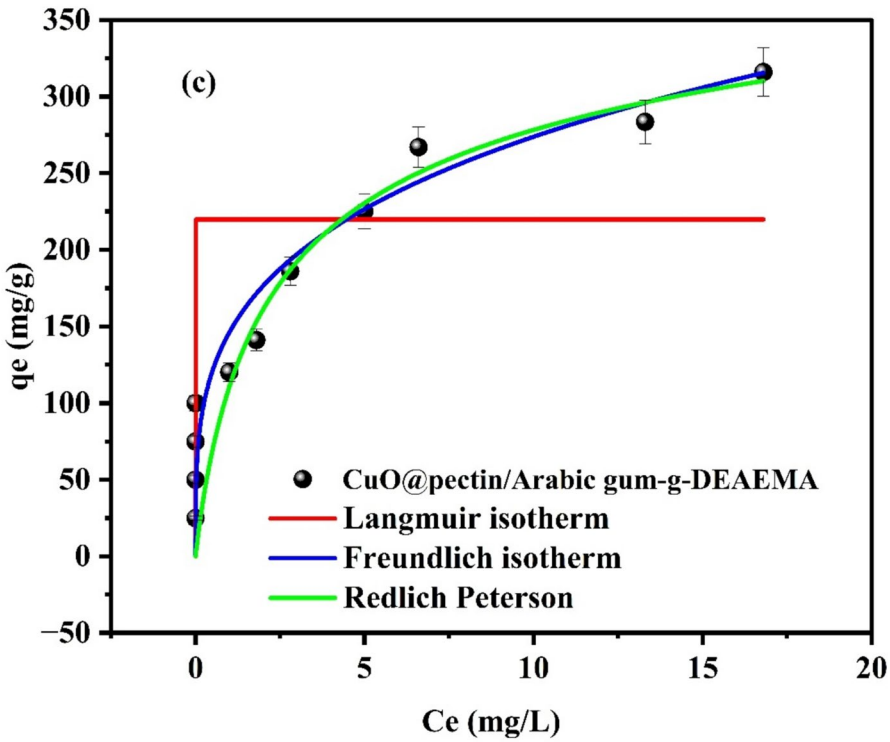

Table 2 Kinetic parameters for MB dye adsorption

Model	Parameter	pectin/Arabic gum-g-DEAEMA	CuO@pectin/Arabic gum-g-DEAEMA
	q_e exp. (mg/g)	187.5	225
PFO	Equation	$q_t = q_e\left(1 - e^{-k_1 t}\right)$	
	q_e(mg/g)	207.58 ± 13.05	230.18 ± 3.30
	k_1(min^{-1})	0.02203 ± 0.0029	0.04968 ± 0.0045
	Reduced Chi-Sqr	200.11	31.21
	R^2	0.94752	0.99453
PSO	Equation	$q_t = \frac{k_2 q_e^2 t}{1+k_2 q_e t}$	
	q_e(mg/g)	240.56 ± 14.86	256.56 ± 10.54
	k_2(g/mg·min)	1.26515×10^{-4}	3.2024×10^{-4}
	Reduced Chi-Sqr	61.38	83.96
	R^2	0.98912	0.98529

value) also indicate that the introduction of CuO nanoparticles improves the hydrogel's ability to remove MB dye efficiently.

The findings confirm that the adsorption of MB dye onto both hydrogels is best described by the pseudo-second-order kinetic model, suggesting that the process is mainly controlled by chemisorption mechanisms involving electrostatic interactions and surface complexation (Yousry et al., 2025). The CuO@pectin/Arabic gum-g-DEAEMA hydrogel exhibits superior adsorption capacity and faster kinetics, demonstrating its potential as an efficient adsorbent for wastewater treatment applications.

3.9 Isotherm Study

The adsorption isotherms for adsorption of MB dye onto pectin/Arabic gum-g-DEAEMA biohydrogel and CuO@pectin/Arabic gum-g-DEAEMA nanocomposite hydrogel were studied using the Langmuir, Freundlich, and Redlich-Peterson models, as shown in Fig. 7b and c. The model parameters and fitting accuracy for each system are summarized in Table 3.

For the pectin/Arabic gum-g-DEAEMA biohydrogel, the isotherm parameters suggest the following observations:

- Langmuir Model: The maximum adsorption capacity (q_{max}) was 275.81 mg/g, with an adsorption affinity constant (k_L) of 0.12008 L/mg. However,

Table 3 Isotherm model parameters for MB Dye adsorption

Model	Parameter	Pectin/Arabic Gum-g-DEAEMA	CuO@Pectin/Arabic Gum-g-DEAEMA
Langmuir	Equation	$q_e = \frac{q_{max} K_L C_e}{1+K_L C_e}$	
	q_{max} (mg/g)	275.81	219.82
	K_L (L/mg)	0.12008	−5.09E45 (poor fit)
	R^2	0.78088	0.47837
	$\chi 2$	5736	1236
Freundlich	Equation	$q_e = K_F C_e^{1/n_f}$	
	K_f (mg/g)	61.76	145.96
	n_f	2.68	3.66 ± 0.46
	R^2	0.84682	0.99989 (Best fit)
	$\chi 2$	1.25	864
Redlich-Peterson	Equation	$q_e = \frac{K_R C_e}{1+a_R C_e^g}$	
	a_R	372147.61	194.96
	K_R	10009.20	0.76476
	g	0.45065	0.89511
	R^2	0.93615 (Best fit)	0.8031
	$\chi 2$	2436	415

the R^2 value of 0.78088 indicates a moderate fit, and the high reduced Chi-square ($\chi 2 = 1236.14$) suggests some deviation from monolayer adsorption behavior (Al-Gorair et al., 2022).

- Freundlich Model: The adsorption intensity factor (n_f) was 2.68, indicating favorable adsorption. The Freundlich constant (k_f) was 61.76 mg/g. The higher R^2 value of 0.84682 compared to Langmuir suggests that adsorption follows a multilayer mechanism with heterogeneous surface adsorption (Hussain et al., 2025).
- Redlich-Peterson Model: This model, which combines features of both Langmuir and Freundlich, yielded an R^2 value of 0.93615, indicating the best fit among the three models. The model parameter $g = 0.45065$ suggests a deviation from ideal Langmuir behavior, reinforcing the presence of heterogeneous adsorption sites (Mahmoud et al., 2023).

For the CuO@pectin/Arabic gum-g-DEAEMA nanocomposite hydrogel, significant differences in adsorption behavior were observed:

- Langmuir Model: The maximum adsorption capacity (q_{max}) was 219.82 mg/g, but the adsorption affinity constant (K_L) showed an unrealistic negative value, indicating poor model fitting ($R^2 = 0.47837$). This suggests that the Langmuir model is not suitable for describing the adsorption process for the CuO-modified hydrogel.
- Freundlich Model: The model provided an excellent fit, with an R^2 value of 0.99989, indicating a strong multilayer adsorption behavior. The adsorption intensity factor ($n_f = 3.66$) suggests stronger adsorption compared to the unmodified hydrogel. The Freundlich constant ($K_f = 145.96$ mg/g) was significantly higher than that for the unmodified hydrogel, showing that the CuO modification enhances adsorption efficiency.
- Redlich-Peterson Model: This model also provided a good fit ($R^2 = 0.8031$), but with a higher reduced Chi-square ($\chi 2 = 2436.04$), indicating deviations at higher concentrations. The value of $g = 0.89511$ suggests that the model approaches Langmuir-like behavior at higher concentrations.

The CuO@pectin/Arabic gum-g-DEAEMA hydrogel exhibited superior adsorption capacity and affinity compared to the pectin/Arabic gum-g-DEAEMA hydrogel. The Freundlich model provided the best fit for the CuO-modified hydrogel, confirming that adsorption occurs through multilayer interactions on a heterogeneous surface. The Redlich-Peterson model

best described the adsorption behavior of the pectin/Arabic gum-g-DEAEMA hydrogel, suggesting a combination of monolayer and multilayer adsorption mechanisms.

The CuO incorporation enhanced the adsorption performance of the biohydrogel, increasing the adsorption capacity and improving surface interactions. The adsorption followed a heterogeneous, multilayer mechanism, as indicated by the strong agreement with the Freundlich isotherm. These results suggest that CuO@pectin/Arabic gum-g-DEAEMA hydrogels can be effectively used for MB dye removal in wastewater treatment applications.

3.10 Adsorption Mechanism of Methylene Blue

The adsorption mechanism of methylene blue (MB) onto pectin/Arabic gum-g-DEAEMA biohydrogel and CuO@pectin/Arabic gum-g-DEAEMA nanocomposite hydrogel was interpreted based on the kinetic, isotherm, and structural analyses, as illustrated schematically in Fig. 8. The obtained kinetic results revealed that the adsorption process follows the pseudo-second-order (PSO) model, indicating that chemisorption is the dominant adsorption mechanism involving electron sharing or exchange between the adsorbent surface and MB molecules (Verma et al., 2026a).

The Freundlich isotherm model provided the best fit for the CuO-loaded nanocomposite hydrogel, suggesting heterogeneous multilayer adsorption on energetically non-uniform surfaces. In contrast, the pristine pectin/Arabic gum-g-DEAEMA hydrogel exhibited mixed adsorption characteristics, indicating the coexistence of monolayer and multilayer adsorption processes. These findings indicate that the incorporation of CuO nanoparticles generated additional adsorption-active sites and increased surface heterogeneity.

The adsorption of MB onto the developed hydrogel systems mainly occurs through multiple synergistic interactions. Electrostatic attraction plays an important role due to the interaction between the cationic MB dye molecules and negatively charged functional groups such as carboxylate groups ((–COO^-)) present in pectin and Arabic gum chains. Hydrogen bonding may also occur between MB molecules and hydroxyl ((–OH)), carboxyl ((–COOH)), and amine-containing groups within the hydrogel network.

Additionally, π–π stacking interactions can occur between the aromatic rings of methylene blue and

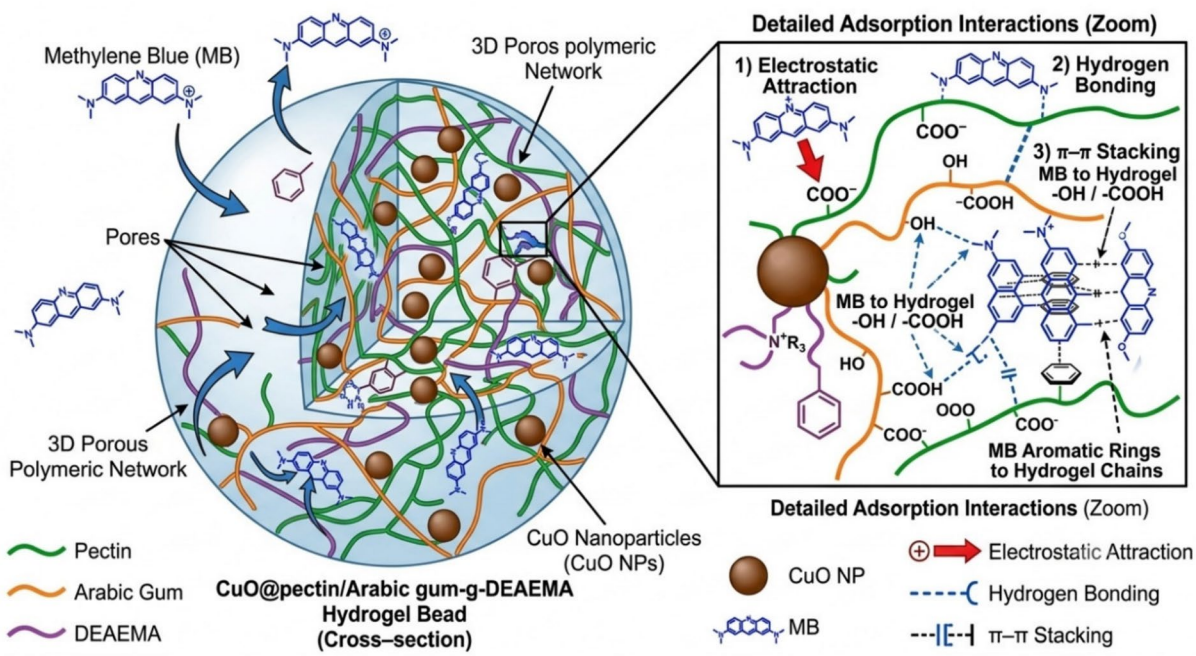

Fig. 8 Proposed adsorption mechanism of methylene blue (MB) onto CuO@pectin/Arabic gum-g-DEAEMA nanocomposite hydrogel

the polymeric chains of the hydrogel matrix, contributing to stronger adsorption affinity. The incorporation of CuO nanoparticles further enhanced adsorption through surface coordination interactions and by increasing the available surface area and pore accessibility. The BET and NLDFT analyses confirmed the mesoporous structure of the nanocomposite hydrogel, which facilitates dye diffusion and improves mass transfer within the porous network.

The enhanced adsorption performance of the CuO@pectin/Arabic gum-g-DEAEMA nanocomposite hydrogel compared with the pristine hydrogel can therefore be attributed to the synergistic effect of improved porosity, increased adsorption-active sites, and the coexistence of electrostatic attraction, hydrogen bonding, π–π stacking, and CuO-assisted surface interactions. Similar adsorption behavior and multifunctional interaction mechanisms have recently been reported for hydrogel-based adsorbents in wastewater remediation applications (Sharma et al., 2026).

A comparison between the adsorption performance of the developed CuO@pectin/Arabic gum-g-DEAEMA nanocomposite hydrogel and previously reported adsorbents for methylene blue (MB) removal is presented in Table 4. The developed nanocomposite hydrogel exhibited a maximum adsorption capacity (q_m) of 275.81 mg g^{-1}, which is significantly higher than many recently reported adsorbent systems, including CuO NCs/CMC (100 mg g^{-1}), pectin-modified @CuO (132.27 mg g^{-1}), XGmMAN-3@CuO nanocomposite (144.5 mg g^{-1}), and $AgTiO_2$@AG-g-P(AM-co-AN) hydrogel (104.5 mg g^{-1}).

The superior adsorption performance of the developed hydrogel can be attributed to the synergistic combination of the mesoporous hydrogel network, the abundance of functional groups originating from pectin, Arabic gum, and DEAEMA, as well as the incorporation of CuO nanoparticles, which provide additional adsorption-active sites and improve surface heterogeneity. Moreover, the gamma irradiation–induced synthesis route contributed to the formation of a uniform crosslinked structure with enhanced porosity and structural stability, facilitating efficient dye diffusion and adsorption.

4 Conclusion

In this study, pectin/Arabic gum-g-DEAEMA hydrogels and CuO@pectin/Arabic gum-g-DEAEMA nanocomposite hydrogels were successfully synthesized via gamma irradiation-induced copolymerization as a clean, initiator-free alternative to conventional chemical synthesis methods. Structural and physicochemical characterizations confirmed the successful grafting of DEAEMA and the effective incorporation of CuO nanoparticles into the hydrogel matrix. The incorporation of CuO nanoparticles improved the thermal stability, surface morphology, and porous structure of the hydrogel. BET analysis showed an increase in surface area from 14.05 to 28.22 m^2 g^{-1}, while the total pore volume increased from 0.08685 to 0.2201 cm^3 g^{-1}, confirming enhanced porosity and greater accessibility of adsorption sites. These textural improvements contributed to the enhanced methylene blue adsorption performance of the nanocomposite hydrogel. Adsorption kinetic studies showed that the adsorption process followed the pseudo-second-order model, indicating chemisorption as the dominant mechanism. Isotherm analysis revealed that the CuO-loaded nanocomposite hydrogel followed the Freundlich model, suggesting

Table 4 Comparison of the maximum adsorption capacity (q_m mg/g) of CuO@pectin/Arabic gum-g-DEAEMA nanocomposite hydrogel with previously reported adsorbents for methylene blue dye removal from aqueous solutions

Adsorbent	(q_m mg/g)	Ref. no
CuO NCs/CMC	100	(Albokheet and Alfaiyz, 2021)
pectin-modified @CuO	132.27	(Kumar et al., 2024)
XGmMAN-3@CuO NCs	144.5	(Yadav et al., 2025)
CL-GA/Fe3O4	209.8	(Farsijani & Nojavan, 2024)
CA/GA/ES	29.71	(Sandikci & Isik, 2025)
$AgTiO_2$@AG-g-P(AM-co-AN)	104.5	(Taha et al., 2021)
CuO@pectin/Arabic gum-g-DEAEMA	275.81	Present study

heterogeneous multilayer adsorption, whereas the pristine hydrogel showed mixed adsorption behavior. The CuO@pectin/Arabic gum-g-DEAEMA nanocomposite hydrogel achieved a maximum adsorption capacity of 275.81 mg g^{-1}, exceeding several previously reported adsorbents. In addition to its adsorption performance, the CuO-loaded hydrogel exhibited notable antimicrobial activity, suggesting its potential to reduce biofouling in water treatment applications. Overall, the findings demonstrate that gamma irradiation is an effective strategy for developing multifunctional, biopolymer-based nanocomposite hydrogels with improved adsorption efficiency, porosity, thermal stability, and antimicrobial functionality. These properties make the developed material a promising candidate for sustainable wastewater remediation.

Author Contribution A.S. conceived the study, performed the experimental work, and wrote the main manuscript text. D.M.A. contributed to methodology development, data analysis, and manuscript revision. R.M. assisted in characterization and data interpretation. A.A. contributed to environmental application analysis and discussion. G.A.M. supervised the research, contributed to conceptualization, and reviewed and edited the manuscript. All authors reviewed and approved the final manuscript.

Funding The authors received no specific funding for this work.

Data Availability No datasets were generated or analysed during the current study.

Declarations

Ethical Approval Not applicable. This study does not involve any human participants or animals.

Consent to Participate The authors confirm that all information they provide for this study is realistic experimental data and findings.

Consent to Publish The authors give their consent for the publication of identifiable details, which can include photograph(s) and/or videos and/or case history and/or details within the text ("Material") to be published in the above Journal and Article.

Competing interest The authors declare no competing interests.

References

Abdel-Raouf, M.-S., Farag, R. K., Farag, A. A., Keshawy, M., Abdel-Aziz, A., & Hasan, A. (2023). Chitosan-based architectures as an effective approach for the removal of some toxic species from aqueous media. *ACS Omega, 8*, 10086–10099.

Abdollahi, Z., Zare, E. N., Salimi, F., Goudarzi, I., Tay, F. R., & Makvandi, P. (2021). Bioactive carboxymethyl starch-based hydrogels decorated with CuO nanoparticles: Antioxidant and antimicrobial properties and accelerated wound healing in vivo. *International Journal of Molecular Sciences, 22*, 2531.

Albokheet, W. A., & Alfaiyz, M. G. Y. (2021). Removal of methylene blue dye using copper oxide/carboxymethyl cellulose nanocomposite: Kinetic, equilibrium and thermodynamic studies. *Asian Journal of Advances in Research, 4*, 380–397.

Al-Gethami, W., Qamar, M. A., Shariq, M., Alaghaz, A.-N.M., Farhan, A., Areshi, A. A., & Alnasir, M. H. (2024). Emerging environmentally friendly bio-based nanocomposites for the efficient removal of dyes and micropollutants from wastewater by adsorption: A comprehensive review. *RSC Advances, 14*, 2804–2834.

Al-Gorair, A. S., Sayed, A., & Mahmoud, G. A. (2022). Engineered superabsorbent nanocomposite reinforced with cellulose nanocrystals for remediation of basic dyes: Isotherm, kinetic, and thermodynamic studies. *Polymers, 14*, 567.

Al-Hazmi, G. H., Refat, M. S., & Shahat, A. (2022). Adsorption of organic dye onto mesoporous aluminosilica monoliths: Equilibrium, kinetic and thermodynamic studies. *ChemistrySelect, 7*, Article e202201995.

Ali, T., Li, Y., Fang, B., Raza, S., & Xiao, Y. (2026). Interfacial charge-transfer in CoAl-LDH/CoOx for photocatalytic dye degradation and UV/H2O2 assisted real-wastewater treatment. *Journal of Materials Chemistry C, 14*, 2721–2735.

Alkhaldi, H. S., Baata, M., Alhajri, F., Elbasiony, A. M., Almoiqli, M. S., Madani, M., & Ghobashy, M. M. (2026). Recent progress in the preparation and environmental applications of functionalized adsorbent hydrogel: A review. *RSC Advances, 16*, 7287–7336.

Al-Mur, B. A., & Jamal, M. T. (2026). Eco-friendly dye removal using chitosan: Characterization and kinetic modeling of methylene blue and methyl orange adsorption. *Polymers, 18*, Article 546.

Biswal, T. (2024). Pectin-based biocomposite materials for biomedical and cosmetic applications. *Biopolymers in Pharmaceutical and Food Applications, 2*, 471–495.

Deo, K. A., Lokhande, G., & Gaharwar, A. K. (2019). Nanostructured hydrogels for tissue engineering and regenerative medicine. *Encyclopedia of Tissue Engineering and Regenerative Medicine, 1*, 3.

Eldondaity, L. S., Sayed, A., Ahmed, H. M., Qassim, M. I., Shoukry, E. M., Abdel-Geleel, M., & Mahmoud, G. A. (2026). Sustainable bandgap engineering via oxalate-driven synthesis of tin oxide heterostructures for enhanced visible-light photocatalysis in aqueous waste treatment. *Materials Science and Engineering: B, 330*, Article 119483.

El-Kousy, S. M., El-Shorbagy, H. G., & El-Ghaffar, M. A. A. (2020). Chitosan/montmorillonite composites for fast removal of methylene blue from aqueous solutions. *Materials Chemistry and Physics, 254*, Article 123236.

Ellis, G. J., & Martin, M. C. (2016). Opportunities and challenges for polymer science using synchrotron-based infrared spectroscopy. *European Polymer Journal, 81*, 505–531.

Elwakeel, K. Z. (2009). Removal of reactive black 5 from aqueous solutions using magnetic chitosan resins. *Journal of Hazardous Materials, 167*, 383–392.

Fakry, H., Salama, E., Taha, A., Ossman, M., Bonanomi, G., Abd-ElGawad, A. M., & El-Amier, Y. A. (2026). Sustainable methylene blue dye removal via bio-derived micro/micron-sized porous particles *Zygophyllum coccineum* and *Calotropis procera*: A machine learning-assisted study. *Scientific Reports, 16*, Article 10984.

Farsijani, A., & Nojavan, S. (2024). Removal of Cationic Dyes from Aqueous Samples Using Magnetic Gum Arabic Polymer. *Advanced Environmental Sciences, 22*(3), 537-556. https://doi.org/10.48308/envs.2024.1400

Gao, B., Yu, H., Wen, J., Zeng, H., Liang, T., Zuo, F., & Cheng, C. (2021). Super-adsorbent poly (acrylic acid)/laponite hydrogel with ultrahigh mechanical property for adsorption of methylene blue. *Journal of Environmental Chemical Engineering, 9*, Article 106346.

Guan, G., Zhang, L., Zhu, J., Wu, H., Li, W., & Sun, Q. (2021). Antibacterial properties and mechanism of biopolymer-based films functionalized by CuO/ZnO nanoparticles against *Escherichia coli* and *Staphylococcus aureus*. *Journal of Hazardous Materials, 402*, Article 123542.

Hamze, Z. K., Faraj, M., Mhanna, R., Younes, G., & El-Dakdouki, M. H. (2024). Corrosion inhibition efficiency of biosynthesized silver nanoparticles using *Citrus aurantium* peels extract. *Journal of Bio- and Tribo-Corrosion, 10*, 56.

Huang, X., Zheng, J., Zhou, J., Wu, Y., Wang, J., Raza, S., Liu, P., Wang, W.-J., & Shi, S. (2026). Recent advances in transition metal-catalyzed ethylene/polar olefin copolymerization. *Coordination Chemistry Reviews, 548*, 217147.

Hussain, N., Asif, M., Shafaat, S., Khan, M. S., Riaz, N., Iqbal, M., Javed, A., Butt, T. A., Shaikh, A. J., & Bilal, M. (2025). Multilayer adsorption of reactive orange 16 dye onto Fe_2O_3/ZnO hybrid nanoadsorbent: Mechanistic insights from kinetics, isotherms and dynamic light scattering studies. *Journal of Chemical Technology and Biotechnology, 100*, 50–66.

Joshi Navare, K., Eggermont, L. J., Rogers, Z. J., Mohammed, H. S., Colombani, T., & Bencherif, S. A. (2020). Antimicrobial hydrogels: Key considerations and engineering strategies for biomedical applications. *Racing for the surface: Pathogenesis of implant infection and advanced antimicrobial strategies* (pp. 511–542)

Khozemy, E. E., Nasef, S. M., & Mahmoud, G. A. (2018). Synthesis and characterization of antimicrobial nanocomposite hydrogel based on wheat flour and poly (vinyl alcohol) using γ-irradiation. *Advances in Polymer Technology, 37*, 3252–3261.

Koshy, J. T., Kalumkumvathukkal Sajeev, S., John, A. S., & Sangeetha, D. (2026). Development of a pH-responsive nanoantibiotic hydrogel system based on PVA/pectin and biomass-derived bacterial nanocellulose for antibacterial wound dressings. *ACS Applied Bio Materials, 9*, 1425–1449.

Krishna, D., Sankar, M., Sarma, P., & Samundeshwari, E. (2024). Copper nanoparticles loaded gelatin/polyvinyl alcohol/guar gum-based 3D printable multimaterial hydrogel for tissue engineering applications. *International Journal of Biological Macromolecules*. https://doi.org/10.1016/j.ijbiomac.2024.133866

Kumar, R., Pande, P. P., Chaurasiya, A., Dey, K. K., Kushwaha, N., Kumar, P., & Kashaudhan, K. (2025). Synthesis and characterization of novel pectin-based copper oxide nanocomposite and its application for removal and photocatalytic degradation of methylene blue from aqueous solution. *Iranian Polymer Journal, 34*(1), 65-81. https://doi.org/10.1007/s13726-024-01355-0

Levien, M., Amin, I., de Paula Kodaira, F. V., & Weltmann, K.-D. (2023). Direct grafting of microwrinkled hydrogels by atmospheric-pressure plasma polymerization: Going simple and environmentally friendly. *European Polymer Journal, 198*, 112413.

Mahmoud, G., Abdel Khalek, M., Shoukry, E., Amin, M., & Abdulghany, A. (2019). Removal of phosphate ions from wastewater by treated hydrogel based on chitosan. *Egyptian Journal of Chemistry, 62*, 1537–1549.

Mahmoud, G. A., Sayed, A., Thabit, M., & Safwat, G. (2020). Chitosan biopolymer based nanocomposite hydrogels for removal of methylene blue dye. *SN Applied Sciences, 2*, 968.

Mahmoud, G. A., Sayed, A., Abdel-raouf, M.E.-S., Danial, M. Y. F., & Amin, A. (2023). Efficient removal of Cr(VI) from aqueous solutions using chitosan/Na-alginate biobased nanocomposite hydrogel. *Journal of Applied Polymer Science, 140*, e53886.

Mallakpour, S., Azadi, E., & Hussain, C. M. (2020). Environmentally benign production of cupric oxide nanoparticles and various utilizations of their polymeric hybrids in different technologies. *Coordination Chemistry Reviews, 419*, 213378.

Martínez-Sabando, J., Coin, F., Melillo, J. H., Goyanes, S., & Cerveny, S. (2023). A review of pectin-based material for applications in water treatment. *Materials (Basel, Switzerland), 16*, 2207.

Mashhadi, R., Nourmohammadi, J., & Tavakol, M. (2026). Enzymatically crosslinked pectin–silk fibroin hydrogel with embedded ZnO@Gallic acid nanoparticles: An injectable, self-healing, and antibacterial wound dressing. *International Journal of Biological Macromolecules, 349*, 150823.

Metwally, S. E., Farrag, H. A. A., Abd El-Rehim, H. A., Shamma, R. N., Ali, A. E., & Helmy, O. M. (2026). The antimicrobial peptide EM86 loaded to gamma-irradiated sodium alginate/polyvinyl alcohol electrospun nanofibrous dressing treated multidrug-resistant *Pseudomonas aeruginosa* wound infections in BALB/c mice. *Frontiers in Bioengineering and Biotechnology, 14*, 1776154.

Miralaei, N., Mohammadimehr, M., Farazin, A., Ghasemi, A. H., & Bargozini, F. (2023). Design, fabrication, evaluation, and in vitro study of green biomaterial and antibacterial polymeric biofilms of polyvinyl alcohol/tannic acid/CuO/SiO2. *Journal of the Mechanical Behavior of Biomedical Materials, 148*, 106219.

Mohamed, T. M., Sayed, A., & Mahmoud, G. A. (2023). Tuning of the properties of polyvinyl alcohol/polyacrylamide film by phytic acid and gamma radiation crosslinking for food packaging applications. *Polymer-Plastics Technology and Materials, 62*, 866–876.

Nezhad-Mokhtari, P., Hamishehkar, H., Farahpour, M. R., Mehdipour, A., Rahbarghazi, R., Milani, M., & Mehrali, M. (2024). Engineered bioadhesive self-healing nanocomposite hydrogel to fight infection and

accelerate cutaneous wound healing. *Chemical Engineering Journal, 489*, 150992.

Othman, N. A. F., Selambakkannu, S., Yamanobe, T., Hoshina, H., Seko, N., & Abdullah, T. A. T. (2020). Radiation grafting of DMAEMA and DEAEMA-based adsorbents for thorium adsorption. *Journal of Radioanalytical and Nuclear Chemistry, 324*, 429–440.

Oun, A. A., & Rhim, J.-W. (2017). Carrageenan-based hydrogels and films: Effect of ZnO and CuO nanoparticles on the physical, mechanical, and antimicrobial properties. *Food Hydrocolloids, 67*, 45–53.

Qumar, U., Hassan, J. Z., Bhatti, R. A., Raza, A., Nazir, G., Nabgan, W., & Ikram, M. (2022). Photocatalysis vs adsorption by metal oxide nanoparticles. *Journal of Materials Science & Technology, 131*, 122–166.

Rahman, M. M., & Rimu, S. H. (2022). Recent development in cellulose nanocrystal-based hydrogel for decolouration of methylene blue from aqueous solution: A review. *International Journal of Environmental Analytical Chemistry, 102*, 6766–6783.

Raza, S., Rehman, A. U., Zhao, Z., Li, H., Chen, C., Yu, W., Liu, Y., Xu, Y., Shen, L., & Lin, H. (2026). Triatomic-doped MXene based catalyst with sodium alginate encapsulation their molecular and DFT calculation study for efficient photocatalytic removal of disinfected by-product from drinking water. *Chemical Engineering Journal, 530*, 173462.

Sabry, R., Sayed, A., El-Sayed, I. E. T., & Mahmoud, G. A. (2025). Optimizing pectin-based biofilm properties for food packaging via E-beam irradiation. *Radiation Physics and Chemistry, 229*, 112474.

Sahai, A., Goswami, N., Mishra, M., & Gupta, G. (2018). Structural, vibrational and electronic properties of CuO nanoparticles synthesized via exploding wire technique. *Ceramics International, 44*, 2478–2484.

Sandikci, M., & Isik, B. (2025). Fabrication of calcium alginate/gum Arabic/egg shell composite microbeads for adsorptive removal of methylene blue dye from aqueous solutions. *Macromolecular Research*. https://doi.org/10.1007/s13233-025-00408-4

Sayed, A., Hany, F., Abdel-Raouf, M.E.-S., & Mahmoud, G. (2022a). Gamma irradiation synthesis of pectin- based biohydrogels for removal of lead cations from simulated solutions. *Journal of Polymer Research*. https://doi.org/10.1007/s10965-022-03219-8

Sayed, A., Yasser, M., Abdel-raouf, M.-s, & Mohsen, R. (2022b). Green starch/graphene oxide hydrogel nanocomposites for sustained release applications. *Chemical Papers, 76*, 5119–5132.

Sayed, A., Behalo, M., Feteha, A., Younis, A., Keshawy, M., Yousry, R., & Abdel-Raouf, M. E. (2025). Unveiling the removal performance of banana peel biochar and rice husk nanoparticles for crystal violet and methylene blue dyes from aqueous media. *Discover Environment, 3*, 143.

Sayed, A., Emad, T., Badawi, S., Mahmoud, G. A., & Abdel-Raouf, M.-S. (2025b). Gamma-irradiated chitosan-HPMC/*Ulva lactuca* based hydrogel for heavy metal remediation from aqueous solutions. *International Journal of Biological Macromolecules, 320*, Article 146130.

Sayed, A., Hiekal, A. S., Moussa, S. I., Aydia, M. I., El-Sabagh, H. A., Mahmoud, G. A., Amin, A. M., & El-Azony, K. M. (2025c). Preparation and characterization of silver ferrite nanoparticles ($AgFeO_2$) and investigation of their cytotoxicity properties. *BioNanoScience, 15*, 353.

Sayed, A., Mahmoud, G. A., Haggag, E.-S.A., & Salem, A. R. (2026). A novel xerogel based on modified cellulose acetate propionate for the selective removal of uranium(VI) ions. *Surfaces and Interfaces*. https://doi.org/10.1016/j.surfin.2026.109386

Shang, H., Ma, C., Li, C., Zhao, J., Elmer, W., White, J. C., & Xing, B. (2021). Copper oxide nanoparticle-embedded hydrogels enhance nutrient supply and growth of lettuce (*Lactuca sativa*) infected with *Fusarium oxysporum* f. sp. *lactucae*. *Environmental Science & Technology, 55*, 13432–13442.

Sharma, G., Verma, Y., Dhiman, P., Wang, T., Jain, S., García-Peñas, A., & Lai, C. W. (2026). Gellan gum–alginate/PVA-co-PAM crosslinked hydrogel for phenol adsorption: Fabrication, characterization, and performance. *International Journal of Biological Macromolecules, 350*, 150967.

Sun, S.-F., Wan, H.-F., Zhao, X., Gao, C., Xiao, L.-P., & Sun, R.-C. (2023). Facile construction of lignin-based network composite hydrogel for efficient adsorption of methylene blue from wastewater. *International Journal of Biological Macromolecules, 253*, 126688.

Taha, G. M., Mansor, E., & Sultan, M. (2021). Development of Arabic gum-based AgTiO2 nanocomposite hydrogel as high efficient adsorbent of cationic dye methylene blue from water. *International Journal of Biological Macromolecules, 193*, 1859–1870.

Taktak, F. F., & Şimşek, S. (2022). Exploring the adsorption performance of gum xanthan/poly (acrylic acid-co-2-(diethlyamino)ethyl methacrylate) based adsorbent toward cationic and anionic dyes. *Journal of Macromolecular Science, Part b: Physics, 61*, 1282–1301.

Thapliyal, D., Verros, G. D., & Arya, R. K. (2025). Nanoparticle-doped antibacterial and antifungal coatings. *Polymers, 17*, 247.

Uneputty, A., Dávila-Lezama, A., Garibo, D., Oknianska, A., Bogdanchikova, N., Hernández-Sánchez, J., & Susarrey-Arce, A. (2022). Strategies applied to modify structured and smooth surfaces: A step closer to reduce bacterial adhesion and biofilm formation. *Colloid and Interface Science Communications, 46*, 100560.

Verma, A., Dhiman, P., Lai, C. W., García-Peñas, A., & Sharma, G. (2026a). Fabrication and characterization of corn-silk biochar@Fe3O4 composite for the adsorption of malachite green dye. *Waste Disposal & Sustainable Energy, 8*, 159–178.

Verma, Y., Verma, A., Sharma, J., Dhiman, P., Naushad, M., Wang, T., García- Peñas, A., & Sharma, G. (2026b). Green hydrogel as sustainable adsorbents: Bridging biopolymer & environmental remediation. *Advanced Industrial and Engineering Polymer Research*. https://doi.org/10.1016/j.aiepr.2026.03.003

Wang, W., Ni, J., Chen, L., Ai, Z., Zhao, Y., & Song, S. (2020). Synthesis of carboxymethyl cellulose-chitosan-montmorillonite nanosheets composite hydrogel for dye effluent

remediation. *International Journal of Biological Macromolecules, 165*, 1–10.

Wu, S., Li, H., Futaba, D. N., Chen, G., Chen, C., Zhou, K., Zhang, Q., Li, M., Ye, Z., & Xu, M. (2022). Structural design and fabrication of multifunctional nanocarbon materials for extreme environmental applications. *Advanced Materials, 34*, Article 2201046.

Yadav, L., & Yadav, L. (2005). Infrared (IR) spectroscopy. *Organic spectroscopy* (pp. 52–106)

Yadav, V., Pande, P. P., Chaurasiya, A., Rai, S., Chaudhary, A., & Kashaudhan, K. (2025). Fabrication and analysis of copper oxide–based hydrogel nanocomposite for the extraction of MB dye from wastewater. *Colloid and Polymer Science, 303*, 1721–1742.

Yadollahi, M., Gholamali, I., Namazi, H., & Aghazadeh, M. (2015). Synthesis and characterization of antibacterial carboxymethylcellulose/CuO bio-nanocomposite hydrogels. *International Journal of Biological Macromolecules, 73*, 109–114.

Yang, H., Yin, S., Zhang, P., Zheng, Q., Raza, S., Li, D., & Sui, Y. (2025). Hydrothermal synthesis of MnCO3 and metal-organic frameworks on MXene surface incorporated in sodium alginate hydrogel for efficient removal of disinfection byproducts. *Separation and Purification Technology, 365*, Article 132600.

Yousry, R., Sayed, A., Behalo, M. S., Abdel-raouf, M. E., & Feteha, A. (2025). Tailoring of carboxymethyl guar gum hydrogels via gamma irradiation for remarkable removal of cationic and anionic dyes from simulated solutions. *International Journal of Biological Macromolecules, 284*, Article 137867.

Zhang, P., Claudine, U., Raza, S., Zhang, Q., Ye, J., Liu, M., Hayat, A., Bashir, T., Ghasali, E., Sengodan, P., Zhang, R., & Orooji, Y. (2025a). Advanced photocatalytic treatment of aqueous disinfection by-products with sodium alginate hydrogel-encapsulated titanium dioxide and luminous powder: A synergistic mechanism. *Journal of Environmental Chemical Engineering, 13*, 116317.

Zhang, P., Yang, H., Zheng, Q., Nie, G., Abdullah Alzahrani, A. Y., Al-Buriahi, M. S., Alsaiari, N. S., Raza, S., & Orooji, Y. (2025b). Next-generation solar energy: Progress, stability, and prospects of polymer-modified perovskite solar cells; a review. *International Journal of Hydrogen Energy, 106*, 1088–1113.

Zhao, P., Xia, X., Xiao, Y., Ye, Q., Wu, H., Zhu, R., Chen, J., & Qiu, X. (2025). Preparation of quaternary layered double hydroxides from coal gangue and phosphorus tailings for immobilizing Cr(VI) and Cd(II) in contaminated soil. *Colloids and Surfaces a: Physicochemical and Engineering Aspects, 723*, 137340.